Available online at www.sciencedirect.com
SCIENCE DIRECT®
Comput. Methods Appl. Mech. Engrg. 193 (2004) 5143–5175
Computer methods in applied mechanics and engineering
www.elsevier.com/locate/cma

Effective relaxation for microstructure simulations: algorithms and applications

S. Bartels [a], C. Carstensen [b,*], K. Hackl [c], U. Hoppe [c]

[a] Department of Mathematics, University of Maryland, College Park, MD 20742, USA
[b] Department of Mathematics, Humboldt-Universität zu Berlin, Unter den Linden 6, D-10099 Berlin, Germany
[c] Lehrstuhl für Allgemeine Mechanik, Ruhr-Universität Bochum, Universitätsstrasse 150, D-44801 Bochum, Germany

Received 26 June 2003; received in revised form 18 December 2003; accepted 18 December 2003

Abstract

For a wide class of problems in continuum mechanics like those involving phase transitions or finite elastoplasticity, the governing potentials tend to be *not* quasiconvex. This leads to the occurrence of microstructures of in principle arbitrarily small scale, which cannot be resolved by standard discretization schemes. Their effective macroscopic properties, however, can efficiently be recovered with relaxation theory.

The paper introduces the variational framework necessary for the implementation of relaxation algorithms with emphasis on problems with internal variables in a time-incremental setting. The methods developed are based on numerical approximations to notions of generalized convexification. The focus is on the thorough analysis of numerical algorithms and their efficiency in applications to benchmark problems. An outlook to time-evolution of microstructures within the framework of relaxation theory concludes the paper.

Keywords: Computational microstructures; Phase transitions; Multi-scale problems; Adaptive finite element methods; Stabilization; Relaxation; Quasiconvexification

1. Introduction and overview

The variational model of finite elasticity involves concepts such as material objectivity and invertibility which contradicts convexity of the energy density. Rubber-like materials, for instance, lead to polyconvex energy densities that are known to allow classical solutions in Sobolev spaces due to the work of Ball [2].

* Corresponding author.
E-mail addresses: sba@math.umd.edu (S. Bartels), cc@mathematik.hu-berlin.de (C. Carstensen), hackl@am.bi.ruhr-uni-bochum.de (K. Hackl), hoppe@am.bi.ruhr-uni-bochum.de (U. Hoppe).

0045-7825/$ - see front matter © 2004 Published by Elsevier B.V.
doi:10.1016/j.cma.2003.12.065

The direct method of the calculation of variations is in fact based on growth, coercivity, and a generalized convexity condition. This latter quasiconvexity due to Morrey [37] is essentially equivalent to the weak lower semicontinuity of the energy functional. It is a *non-local notion* and extremely difficult to analyze in theory and computation. Therefore, the modern mathematical theory of generalized convexity deals with other, easier notions depicted in the following diagram:

$$\text{convexity} \Rightarrow \text{polyconvexity} \Rightarrow \text{quasiconvexity} \Rightarrow \text{rank-1-convexity}. \tag{1.1}$$

To illustrate the degree of difficulty, we mention that all the aforementioned inclusions are strict and counterexamples are known in general. The fact that rank-1-convexity is *not* equivalent to quasiconvexity was found after decades in [47] and is still left as an open question in 2D! This work is forced to address the aforementioned convexity notions in order to approximate a quasiconvex function numerically within an inner loop over all finite elements for a macroscopic simulation.

Indeed, it appears that time-evolving nonlinear material in finite geometry and a natural time-discretization contradicts the quasiconvexity of the effective energy density [14,15]. This yields to non-existence of solutions in terms of Sobolev functions. Within each time-step, a minimization problem arises in which infimizing sequences (i.e. sequences of deformations which lower the energy but do not approach a minimum in the strong sense) exist but develop enforced higher and higher oscillations on finer and finer length-scales. The weak (but not strong) limit of such infimizing sequences is *not* a classical solution and does not minimize the given energy at all [11].

This paper advertises the use of stabilization, i.e., the introduction of a strictly convex term scaled with a small parameter, for the effective solution of the nonlinear highly dimensional systems of discrete equations for a strong convergence of the macroscopic strains. This is of particular interest in finite elastoplastic problems where internal variables and their time evolution require a pointwise update via nonlinear update formulae such as those needed to model hysteresis [22].

The evaluation of $W^{\mathrm{qc}}(D\mathbf{y}(\mathbf{x}))$ is considered via

(A) Mathematical analysis (provides explicit analytical formulae for W^{qc})
(B) Numerical polyconvexification
(C) Finite-order lamination

For each of those approaches, the numerical treatment is investigated with respect to a proper discretization and an effective solution of the discrete problem. Benchmark examples illustrate computational progress in and difficulties with (A), (B), and (C).

Sections 2–5 are concerned with approach (A) as stated above. Section 2 concerns a scalar 2-well problem and a benchmark example with analytically known generalized solution [16] and adaptive algorithms. A potential with a vectorial 2-well structure,which can be related to the modeling of phase-transitions, follows in Section 3. The numerical solution of the two convexified problems leads to a high-dimensional discrete system of equations. Section 4 is devoted to the analysis of a damped quasi-Newton–Raphson solver and states sufficient conditions for global convergence.

As an example the results of a numerical simulation of a model for phase-transitions in a single-crystal are discussed in Section 5. Here the approach (A) is applicable due to explicit formulae from [31].

Section 6 introduces the general framework associated with approaches (B) and (C) cited above. For this purpose we discuss other notions of convexifications related but different from W^{qc}, which turn out to be more suitable for the application of numerical procedures. Algorithmic issues are discussed and geometrical and mechanical interpretations of the concepts are explained. In Section 7 an application of approach (B) to a two-dimensional Ericksen–James potential is given.

Starting with Section 8 the paper is devoted to inelastic problems related to history-dependent time-evolving material behavior. In the context of inelasticity, relaxation methods have recently been studied in [32,34,41,1,28,27,29]. In this paper, internal variables model the inelastic behavior and monitor the material's intrinsic state. Since relaxation theory was originally developed within the elastic context, the proper treatment of internal variables is a priori less clear.

We put the time-incremental approach from [15] into a more concise variational framework suggested in [35,36]. In Section 9, this concept is applied to a benchmark-problem of single-slip elastoplasticity. We report on efficient procedures of global optimization which allows to calculate relaxations with respect to higher-order laminates. Performing a two-dimensional shear-test we discover a surprising new pattern of higher-order laminated microstructures. A comparison of approaches (B) and (C) applied to the single–slip problem concludes Section 9.

Section 10 finally gives an outlook to the treatment of fully time-dependent evolution of microstructures. Here the update-problem of microstructures and thus measure-valued internal variables has to be solved. We suggest a variational approach involving the Wasserstein-distance between two Young-measures.

2. Non-quasiconvexity, microstructure, and effective energy density

The section addresses microscopic and macroscopic phenomena to explain the relaxation approach and averaged quantities in a simple context; we study the effect of non-convex energy minimization with an energy density W as shown in Fig. 1.

2.1. Non-rank-1-convex minimization problems enforce microstructure

In Fig. 1, the strain F (an $m \times n$ matrix) is a convex combination of two matrices $\mathbf{A}$ and $\mathbf{B}$, i.e. for some volume fraction λ there holds

$$\mathbf{F} = \lambda\mathbf{A} + (1-\lambda)\mathbf{B} \quad \text{for } 0 < \lambda < 1, \tag{2.1}$$

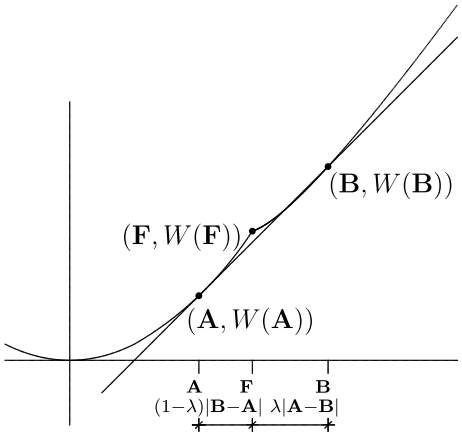

Fig. 1. Non-convex energy density with microstructures depicted in Fig. 2: A hyperplane is tangential at the epigraph of the energy density $W : \mathbb{R}^{m\times n} \to \mathbb{R}$ at the points with the rank-one-connected arguments $\mathbf{A}$ and $\mathbf{B}$ and is strictly below the function at the proper convex combination $\mathbf{F}$.

while, and this is the essential point, the energy $W(\mathbf{F})$ is the pointwise minimum of two quadratic functions and is above the straight line segment at λ, i.e.

$$\lambda W(\mathbf{A}) + (1-\lambda)W(\mathbf{B}) < W(\mathbf{F}). \tag{2.2}$$

The picture in Fig. 1 is essentially one-dimensional but it is meant as some section of a higher-dimensional situation where $\mathbf{F}$ and $\mathbf{A}$, $\mathbf{B}$ belong to $\mathbb{R}^{m\times n}$. We assume a compatibility condition

$$\mathbf{A} = \mathbf{B} + \mathbf{a}\otimes\mathbf{b} \in \mathbb{R}^{m\times n}, \tag{2.3}$$

where $\mathbf{a}$ and $\mathbf{b}$ are vectors with their dyadic product $\mathbf{a}\otimes\mathbf{b}$. In this case, $\mathbf{A}$ and $\mathbf{B}$ are said to be *rank-1-connected*. (Rank-1-connectivity is trivial if either $m = 1$ or $n = 1$ because, then, any two distinct vectors are rank-1-connected; 2.3 is a severe restriction for $m,n \geqslant 2$.)

The non-rank-1-convexity of W means that we can find $\mathbf{A}$, $\mathbf{B}$, $\mathbf{F}$ with (2.1)–(2.3).

According to the diagram 1.1, we observe that the present conditions are sufficient for non-quasiconvexity. Hence we may have non-attainment of minimizers in the model problem

$$\begin{aligned} &\text{Minimize } E(\mathbf{y}) := \int_\Omega W(D\mathbf{y})\,\mathrm{d}\mathbf{x} \text{ among } \mathbf{y}\in\mathscr{A}, \text{ where}\\ &\mathscr{A} := \{\mathbf{y}\in W^{1,p}(\Omega;\mathbb{R}^m):\ \mathbf{y}(\mathbf{x}) = \mathbf{F}\mathbf{x} \text{ for a.e. } \mathbf{x}\in\partial\Omega\}. \end{aligned} \tag{2.4}$$

The exact definition of the Sobolev space $W^{1,p}(\Omega)$ is not important here and the reader might think of Lipschitz continuous deformations $\mathbf{y}$; in general, $W^{1,p}(\Omega)$ consists of all weakly differentiable functions whose first-order partial derivatives are Lebesgue measurable and integrable in its power p. For those functions, the affine boundary condition $\mathbf{y}(\mathbf{x}) = \mathbf{F}\mathbf{x}$ makes sense for almost every boundary point $\mathbf{x}\in\partial\Omega$.

Theorem 2.1. *Suppose (2.1)–(2.4) and let $|\Omega|$ denote the volume of Ω. Then there holds*

$$E_0 := \inf_{\mathbf{y}\in\mathscr{A}} E(\mathbf{y}) \leqslant (\lambda W(\mathbf{A}) + (1-\lambda)W(\mathbf{B}))\,|\Omega| < W(\mathbf{F})\,|\Omega| = E(\mathbf{F}\mathbf{x})$$

(*where* $\mathbf{F}\mathbf{x}$ *also denotes the affine function* $\mathbf{x}\mapsto\mathbf{F}\mathbf{x}$ *in* Ω *prescribed by the boundary values*).

To explore the finer structure in a simple exposition, we consider $n = 2$, $\Omega = (0,1)^2$, and $\mathbf{b} = (0,1)$ in Fig. 2. Given any very small positive parameter ε, let $\mathbf{y}_\varepsilon$ be defined such that the gradient $D\mathbf{y}_\varepsilon$ assumes the values $\mathbf{A}$ and $\mathbf{B}$ according to a layered pattern of $\Omega_\varepsilon := (\varepsilon, 1-\varepsilon)^2$ depicted in Fig. 2 and some intermediate zone in the small frame $\Omega\backslash\Omega_\varepsilon$ to match the boundary conditions to achieve $\mathbf{y}_\varepsilon\in\mathscr{A}$. One can check that this is in fact

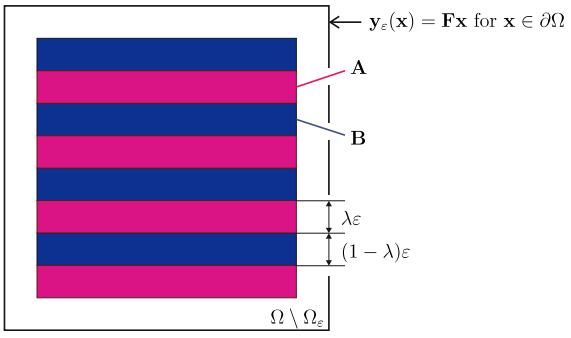

Fig. 2. Domain with microstructure pattern of length-scale ε: The deformation $\mathbf{y}:\Omega\to\mathbb{R}_2$ is globally Lipschitz continuous and is piecewise affine in the interior square $\Omega_\varepsilon := (\varepsilon,1-\varepsilon)^2$ with piecewise constant gradients which equal $\mathbf{B}$ on the depicted dark layers of thickness $(1-\lambda)\varepsilon$ and $\mathbf{A}$ on the others. In the outer frame $\Omega\backslash\Omega_\varepsilon$, $\mathbf{y}$ interpolates between the boundary conditions and values on $\partial\Omega_\varepsilon$.

possible and that $\mathrm{Lip}(\mathbf{y}_\varepsilon)$ is bounded from above by an ε-independent constant and that the distance of $\mathbf{y}_\varepsilon$ to the linear function $\mathbf{Fx}$ tends to zero (in maximum norm) as $\varepsilon \to 0$. It is important to observe that such a construction would be impossible if 2.3 is violated according to Hadamard's jump condition [5].

It is not hard to see that $\lim_{\varepsilon\to 0} E(\mathbf{y}_\varepsilon)$ equals $(\lambda \mathrm{W}(\mathbf{A}) + (1-\lambda)W(\mathbf{B}))|\Omega|$ and this concludes the proof of Theorem 2.1.

2.2. Ill-posed problem

In the absence of exterior forces or other lower order terms, Theorem 2.1 asserts that, the energy is *not* minimized by the linear function $\mathbf{x} \mapsto \mathbf{Fx}$ prescribed by the affine boundary values and, in fact, has no (classical) solution at all!

Theorem 2.2. *Suppose (2.1)–(2.4) and that there exists an affine function $\widetilde{W}$ which assumes the values $W(\mathbf{A})$ and $W(\mathbf{B})$ at $\mathbf{A}$ and $\mathbf{B}$ and is elsewhere a strict lower bound of W,*

$$\begin{aligned} &\widetilde{W}(\mathbf{M}) < W(\mathbf{M}) \quad \text{for all } \mathbf{M} \in \mathbb{R}^{m\times n} \setminus \{\mathbf{A}, \mathbf{B}\}, \quad \text{while} \\ &\widetilde{W}(\mathbf{A}) = W(\mathbf{A}) \quad \text{and} \quad \widetilde{W}(\mathbf{B}) = W(\mathbf{B}). \end{aligned} \tag{2.5}$$

Then, the minimum in (2.4) is not attained, i.e. $E_0 < E(\mathbf{y})$ for any $\mathbf{y} \in \mathscr{A}$.

As a consequence of this non-attainment result, finite element approximations cannot converge strongly (because any strong limit of an infimizing sequence would indeed be a minimizer). Instead, finite element solutions develop oscillations on some scale of the minimal mesh-size and thereby either miss the microstructure (and then are completely misleading) or often become mesh-depending (and are then difficult to compute and quite depending on the solution algorithm). We refer to [33,23,9] for a rigorous analysis of related finite element schemes with a precise characterization of numerical oscillations.

The proof of Theorem 2.2 is by contradiction—so let us consider some $\mathbf{y} \in \mathscr{A}$ with $E_0 = E(\mathbf{y})$. The boundary conditions and an integration by parts show

$$\int_\Omega D\mathbf{y}(\mathbf{x})\,\mathrm{d}\mathbf{x} = \int_{\partial\Omega} D\mathbf{y}(\mathbf{x})\boldsymbol{\nu}(\mathbf{x})\,\mathrm{d}\mathbf{s}_\mathbf{x} = \int_{\partial\Omega} (\mathbf{Fx}) \otimes \boldsymbol{\nu}(\mathbf{x})\,\mathrm{d}\mathbf{s}_\mathbf{x} = \int_\Omega \mathbf{F}\,\mathrm{d}\mathbf{x} = |\,\Omega\,|\,\mathbf{F}.$$

Since the application of the affine $\widetilde{W}$ commutes with integration and since $\widetilde{W} \leqslant W$, this and Theorem 2.1 leads to

$$E(\mathbf{y}) = E_0 \leqslant (\lambda W(\mathbf{A}) + (1-\lambda)W(\mathbf{B}))\,|\,\Omega\,| = \widetilde{W}(\mathbf{F}) = \int_\Omega \widetilde{W}(D\mathbf{y})\,\mathrm{d}x \leqslant \int_\Omega W(D\mathbf{y})\,\mathrm{d}x = E(\mathbf{y})$$

and hence equality of $W(D\mathbf{y})$ and $\widetilde{W}(D\mathbf{y})$. Because of this and since $\widetilde{W}(D\mathbf{y}(\mathbf{x})) \leqslant W(D\mathbf{y}(\mathbf{x}))$ holds for almost all $\mathbf{x} \in \Omega$, we deduce

$$\widetilde{W}(D\mathbf{y}(\mathbf{x})) = W(D\mathbf{y}(\mathbf{x})) \quad \text{for almost every } \mathbf{x} \in \Omega.$$

This and the assumptions 2.5 show that

$$D\mathbf{y}(\mathbf{x}) \in \{\mathbf{A}, \mathbf{B}\} \quad \text{for almost every } \mathbf{x} \in \Omega,$$

that is, the gradient $D\mathbf{y}$ of a Sobolev function $\mathbf{y}$ assumes only two values $\mathbf{A}$ or $\mathbf{B}$. By a result in [5], this is possible only if $\mathbf{A}$ and $\mathbf{B}$ are rank-1-connected (or either $D\mathbf{y} \equiv \mathbf{A}$ or $D\mathbf{y} \equiv \mathbf{B}$) and there are layers where $D\mathbf{y}(\mathbf{x}) = \mathbf{A}$ and those where $D\mathbf{y}(\mathbf{x}) = \mathbf{B}$ separated by parallel straight lines with normal $\mathbf{b}$. In other words, the situation has to be as depicted in Fig. 1. However, there is a problem with the boundary conditions. In fact, on those sides of the domain where the boundary is *not* perpendicular to the direction $\mathbf{b} = (1,0)$, the aforementioned results of [5] show that the (piecewise) constant matrix $D\mathbf{y}$ is rank-1-connected to $\mathbf{F}$ with respect to the direction of the normal $\boldsymbol{\nu} = (0, \pm 1)$. Since $D\mathbf{y}$ allows the values $\mathbf{A}$ and $\mathbf{B}$ along such boundary,

it follows that $\mathbf{A}$ and $\mathbf{B}$ equal $\mathbf{A} = \mathbf{F} + \boldsymbol{\alpha} \otimes (0,1)$ and $\mathbf{B} = \mathbf{F} + \boldsymbol{\beta} \otimes (0,1)$. This and 2.3 for $\mathbf{b} = (1,0)$ lead to the announced contradiction. Hence the infimal energy E_0 is *not* attained.

2.3. Gradient young measures (GYM)

The infimizing sequence $\mathbf{y}_\varepsilon$ is enforced to develop oscillations which are described in terms of mathematical statistics and have a limit which is a measure. In the model example at hand, characteristic statistical variables are $\mathbf{A}$ and $\mathbf{B}$ as well as the volume fraction λ (i.e. the convex coefficient in 2.1). This defines a (*homogeneous*) *gradient Young measure*, abbreviated GYM, which reads

$$\nu = \lambda\delta_{\mathbf{A}} + (1-\lambda)\delta_{\mathbf{B}} \tag{2.6}$$

with a Dirac measure $\delta_{\mathbf{A}}$ supported at the atom $\mathbf{A}$, i.e. the action of ν on a continuous function reads

$$\langle \nu, g\rangle = \lambda g(\mathbf{A}) + (1-\lambda) g(\mathbf{B}) \quad \text{for all } g \in C^0(\mathbb{R}^{m\times n}).$$

[$g \in C^0(\mathbb{R}^{m\times n})$ means $g : \mathbb{R}^{m\times n} \to \mathbb{R}$ is continuous with $\lim_{|\mathbf{M}|\to\infty} g(\boldsymbol{M}) = 0$—this technical detail is not important here.]

Theorem 2.3. *Suppose* (2.1)–(2.3) *and let* $\mathbf{y}_\varepsilon$ *be a Lipschitz continuous function as depicted in Fig.* 2 *and defined in the proof of Theorem* 2.1. *Then any subsequence of* $(\mathbf{y}_\varepsilon)_{\varepsilon>0}$ *generates the Gradient Young Measure* 2.6 *in the sense that the following holds*: *If* ω *is a subdomain of* Ω *and if* $g \in C^0(\mathbb{R}^{m\times n})$ *then*

$$\lim_{\varepsilon\to 0} |\,\omega|^{-1} \int_\omega g(D\mathbf{y}_\varepsilon(\mathbf{x}))\,\mathrm{d}\mathbf{x} = \langle \nu, g\rangle.$$

The proof is simple as for $\varepsilon \to 0$ the domain ω is essentially inside the interior domain Ω_ε and, since the layers of Fig. 2 become finer and finer, leads to $g(D\mathbf{y}_\varepsilon(\mathbf{x})) \in \{g(\mathbf{A}), g(\mathbf{B})\}$ for almost every $\mathbf{x} \in \omega \cap \Omega_\varepsilon$. Moreover, the measure of all $\mathbf{x}$ with $g(D\mathbf{y}_\varepsilon(\mathbf{x})) = g(\mathbf{A})$ and $g(D\mathbf{y}_\varepsilon(\mathbf{x})) = g(\mathbf{B})$ approaches $\lambda|\omega|$ and $(1-\lambda)|\omega|$, respectively. This explains the name volume fraction of λ and concludes the proof.

The theorem motivates the definition of a *Gradient Young Measure* generated by a sequence $(\mathbf{y}_\varepsilon)_{\varepsilon>0}$. The reader may consult the literature [3,4,30,42,48,45,38,50] for further details, proofs and properties of GYMs.

The GYM gives rise to other quantities and relations by evaluation for the test functions g as the energy density, each component of the identity or the derivative of the energy density: The first example yields the *macroscopic energy density*

$$W^{\mathrm{qc}}(\mathbf{F}) := \langle \nu, W\rangle.$$

The center of mass (or expected value) of the GYM leads to the *macroscopic deformation gradient*

$$\mathbf{F} := \langle \nu, \mathbf{Id}\rangle \quad \text{where } \mathbf{Id} \text{ denotes identity.}$$

The continuous derivative DW of the energy density defines the *macroscopic stress*

$$\boldsymbol{\sigma} := \langle \nu, DW\rangle.$$

The deformations $\mathbf{y}_\varepsilon(\mathbf{x})$ are easily seen to converge strongly to the limit $\mathbf{y}(\mathbf{x}) = \mathbf{F}\mathbf{x}$, the *macroscopic deformation*, its gradient $\mathbf{F} = D\mathbf{y}$ is in fact the macroscopic deformation gradient.

In conclusion: The deformation, the macroscopic strain, the stress field, and the GYM are well-defined macroscopic variables we can hope to compute reliably. Other aspects of the microscopic oscillations are not well-posed and we have to expect mesh-depending finite element solutions with defects.

Remark 2.1. The GYM describes some aspects of the oscillations but not all aspects. Fig. 2 illustrates that $\mathbf{A}$, $\mathbf{B}$, and λ are clearly visible, but also the normal $\mathbf{b}$ is important and visible in the figure but not displayed

in the GYM. (In this simple model example, however, **b** is implicitly visible from the calculation 2.3). Nevertheless, the GYM is one macroscopic quantity on the microscopic oscillations.

2.4. Effective energy density and quasiconvexification

The macroscopic energy, also called effective or relaxed energy density, is written in terms of the GYM v as

$$\lim_{\varepsilon\to\infty} |\,\Omega|^{-1}E(\mathbf{y}_\varepsilon) = \langle v, W\rangle =: W^{\mathrm{qc}}(\mathbf{F}).$$

Since $\mathbf{y}_\varepsilon$ is an infimizing sequence, this can be reformulated as

$$W^{\mathrm{qc}}(F) := \inf_{\mathbf{y}(\mathbf{x})=\mathbf{F}\mathbf{x}\text{ for a.e. }\mathbf{x}\in\partial\Omega} |\,\Omega|^{-1}\int_\Omega W(D\mathbf{y}(\mathbf{x}))\,\mathrm{d}\mathbf{x} \tag{2.7}$$

(in the infimum, $\boldsymbol{y}$ is an arbitrary Lipschitz continuous function with the linear boundary values prescribed by $\boldsymbol{Fx}$). The aforementioned function W^{qc} is called the *quasiconvex envelope* of W. A function is called quasiconvex if it coincides with its quasiconvex envelope. In general, the notion of quasiconvex functions is subtle with various difficulties. The question of enforced microstructure is directly linked to the notion of quasiconvexity: Problem 2.4 has a linear solution $\boldsymbol{Fx}$ if and only if $W(\boldsymbol{F}) = W^{\mathrm{qc}}(\boldsymbol{F})$ and there is attainment of microstructure if and only if $W^{\mathrm{qc}}(\boldsymbol{F}) < W(\boldsymbol{F})$.

It is an important observation that the stress fields $\boldsymbol{\sigma}_\varepsilon := DW(D\boldsymbol{y}_\varepsilon)$ of the infimizing sequence $\boldsymbol{y}_\varepsilon$ with GYM v have a limit

$$\boldsymbol{\sigma} := DW^{\mathrm{qc}}(F) = \langle v, DW\rangle.$$

In fact, Fig. 1 illustrates that, since W is smooth at $\boldsymbol{A}$ and $\boldsymbol{B}$, the tangential hyperplane through $(\boldsymbol{A}, W(\boldsymbol{A}))$ and $(\boldsymbol{B}, W(\boldsymbol{B}))$ yields the same stress $\boldsymbol{\sigma} = DW(\boldsymbol{A}) = DW(\boldsymbol{B}) = DW^{\mathrm{qc}}(\boldsymbol{F})$.

This holds true for more general situations [6] and so justifies $\boldsymbol{\sigma}$ as the macroscopic stress field as a local function of the averaged strain $\boldsymbol{F}$. This also underlines the role of the quasiconvex envelope W^{qc} as the effective energy density.

2.5. Well-posed problem

The effective problem on the macroscopic scale reads

$$\text{Minimize}\quad E^{\mathrm{qc}}(\mathbf{y}) := \int_\Omega W^{\mathrm{qc}}(D\mathbf{y}(\mathbf{x}))\,\mathrm{d}\mathbf{x} \text{ among } \mathbf{y}\in\mathscr{A} \tag{2.8}$$

and has a classical solution, namely the linear function $\mathbf{y}(\mathbf{x}) = \mathbf{F}\mathbf{x}$.

In contrast to this, given any macroscopic strain $\mathbf{F} = D\mathbf{y}(\mathbf{x})$ at a material point $\mathbf{x}$, the microscopic problem consists in the calculation of $W^{\mathrm{qc}}(\mathbf{F})$ via 2.7.

In the presence of lower-order terms and more complicated boundary conditions, the rule of thumb is that one needs to quasiconvexify only in the variable of the strain and leaves any other detail as it reads in the original problem to define an effective problem with a classical solution which equals the generalized solution.

More details on the concepts of relaxation theory can be found in [24,37,45]. In this work we focus on a few examples and establish the relaxation and the numerical approximation thereof.

3. Scalar 2-well problem

An anti-plane shear model of phase transitions via the Ericksen–James energy leads to a scalar variational problem with a fourth-order growth energy density $W:\ \mathbb{R}^n \to \mathbb{R}$.

3.1. 2-Well benchmark problem

Given distinct wells $\mathbf{F}_1, \mathbf{F}_2 \in \mathbb{R}^n$, define the scalar 2-well energy density

$$W(\mathbf{F}) = |\,\mathbf{F}-\mathbf{F}_1|^2\,|\,\mathbf{F}-\mathbf{F}_2|^2 \quad \text{for } \mathbf{F}\in\mathbb{R}^n.$$

The benchmark problem on the bounded Lipschitz domain $\Omega \subseteq \mathbb{R}^n$ reads: given $\overline{y}, f \in L^2(\Omega)$ and $y_D \in W^{1-1/p,p}(\partial\Omega)$,

$$\begin{aligned} &\text{Minimize} \quad E(y) := \int_\Omega W(\nabla y)\,\mathrm{d}\mathbf{x} + \|y-\overline{y}\|^2_{L^2(\Omega)} + \int_\Omega fy\,\mathrm{d}\mathbf{x} \text{ among } y\in\mathscr{A},\\ &\text{where} \qquad \mathscr{A} := \{v\in W^{1,4}(\Omega) : v|_{\partial\Omega} = y_D\}. \end{aligned} \tag{3.1}$$

Given $\mathbf{A} = (\mathbf{F}_2-\mathbf{F}_1)/2$ and $\mathbf{B} = (\mathbf{F}_1+\mathbf{F}_2)/2$, the quasiconvex envelope of W equals the convex hull W^{**} of W and is analytically computed in [20],

$$W^{**}(\mathbf{F}) = \max\{|\,\mathbf{F}-\mathbf{B}|^2 - |\,\mathbf{A}|^2, 0\}^2 + 4(|\,\mathbf{A}|^2\,|\,\mathbf{F}-\mathbf{B}|^2 - [\mathbf{A}\cdot(\mathbf{F}-\mathbf{B})]^2) \quad \text{for } \mathbf{F}\in\mathbb{R}^n.$$

It can be shown that the minimum is not attained and that there is a unique generalized solution y with an associated stress field $\boldsymbol{\sigma}$ for which analytic formulae are given in [16].

3.2. Finite element discretization

A discretization of a relaxation of 3.1 is based on a regular triangulation $\mathscr{T}$ of Ω and an approximation $y_{D,h} \in \mathscr{S}^1(\mathscr{T})|_{\partial\Omega}$ of y_D to associate the lowest-order finite element space

$$\mathscr{A}_h = \{v_h \in \mathscr{S}^1(\mathscr{T}) : v_h|_{\partial\Omega} = y_{D,h}\}.$$

Here, $\mathscr{S}^1(\mathscr{T})$ denotes the first-order finite element space on $\mathscr{T}$ (i.e. the set of all elementwise affine, globally continuous functions defined on Ω). The resulting discrete problem is a finite-dimensional convex problem:

$$\text{Minimize } E^{**}(y_h) = \int_\Omega W^{**}(\nabla y_h)\,\mathrm{d}\mathbf{x} + \|y_h-\overline{y}\|^2_{L^2(\Omega)} + \int_\Omega f y_h\,\mathrm{d}\mathbf{x} \text{ among } y_h\in\mathscr{A}_h. \tag{3.2}$$

The numerical analysis of 3.2 given in [20,17] proves convergence $y_h \to y$ in L^2 for $h\to 0$ and a priori and a posteriori error estimates for the distance between the exact unique stress $\boldsymbol{\sigma} = DW^{**}(\nabla y)$ and the discrete stress $\boldsymbol{\sigma}_h = DW^{**}(\nabla y_h)$,

$$\|\boldsymbol{\sigma}-\boldsymbol{\sigma}_h\|_{L^{4/3}(\Omega)} \leqslant C_1 \inf_{v_h\in\mathscr{A}_h} \|y-v_h\|_{W^{1,4}(\Omega)}, \quad \text{and} \quad c_2\eta_M - \text{h.o.t.} \leqslant \|\boldsymbol{\sigma}-\boldsymbol{\sigma}_h\|_{L^{4/3}(\Omega)} \leqslant c_2\eta_M^{1/2} + \text{h.o.t.}$$

The minimal averaging error estimator η_M is defined by

$$\eta_M = \left(\sum_{T\in\mathscr{T}} \eta_T^{4/3}\right)^{3/4} \quad \text{for } \eta_T = \|\boldsymbol{\sigma}_h - \boldsymbol{\sigma}_h^*\|_{L^{4/3}(T)}$$

with the $\boldsymbol{\sigma}_h^* \in \mathscr{S}^1(\mathscr{T})^n$ that minimizes

$$\|\boldsymbol{\sigma}_h - \boldsymbol{\tau}_h\|_{L^{4/3}(\Omega)} \text{ among } \boldsymbol{\tau}_h \in \mathscr{S}^1(\mathscr{T})^n.$$

3.3. Stabilized finite element method

Strong convergence of finite element strain approximations is possible for smooth generalized solutions (e.g. $y \in H^{3/2+\delta}(\Omega)$ for some $\delta > 0$) [7]. Given a regular triangulation $\mathscr{T}$ of mesh-size $h = \max\{\mathrm{diam}(T) : T \in \mathscr{T}\}$ with a finite element space $\mathscr{A}_h$ the stabilized finite element method reads:

$$\begin{aligned} &\text{Minimize } E_h^{**}(y_h) := h\|\nabla y_h\|_{L^2(\Omega)}^2 + \int_\Omega W^{**}(\nabla y_h)\,\mathrm{d}\mathbf{x} + \|y_h - \overline{y}\|_{L^2(\Omega)}^2 + \int_\Omega f y_h\,\mathrm{d}\mathbf{x} \\ &\text{among } y_h \in \mathscr{A}_h. \end{aligned} \tag{3.3}$$

There exist unique finite element solutions y_h of 3.3 which can be calculated with a Newton–Raphson scheme of Section 4.

3.4. Adaptive finite element method

Self-adapting mesh-refining strategies can be employed for the relaxed minimization problem 3.2 based on the aforementioned a posteriori error control.

To approximate the macroscopic quantities in 3.1 we propose the following algorithm with adaptive ($\lambda = 0$) or uniform ($\Theta = 1/2$) mesh refinement and which starts on a coarse initial triangulation $\mathscr{T}_0$ of Ω.

Algorithm 1 (Adaptive algorithm). Input is an initial triangulation $\mathscr{T} = \mathscr{T}_j$ for $j = 0$.

(a) Solve Problem 3.2 (with a Newton–Raphson or quasi-Newton method).
(b) Compute indicators η_T for all $T \in \mathscr{T}$.
(c) Mark element $T \in \mathscr{T}$ (for red-refinement) iff $\Theta \max\{\eta_T : T \in \mathscr{T}\} \leqslant \eta_T$. ($\Theta = 0$ for uniform and $\Theta = 1/2$ for adaptive mesh refining.)
(d) Refine further elements (red–green–blue refinement) to obtain a regular triangulation $\mathscr{T}_{j+1}$ as a refinement of $\mathscr{T}_j$.
(e) Set $j = j + 1$, update $\mathscr{T}$ and go to (a).

3.5. Benchmark example

To illustrate the performance of Algorithm 1 run for the benchmark from [16] with $n = 2$, $\Omega := (0,1) \times (0,3/2)$, $\mathbf{F}_1 = -\mathbf{F}_2 := -(3,2)/\sqrt{13}$, $f \equiv 0$, $\overline{y}(x,y) = f_2(s(x,y) + 1/2)$ for $s(x,y) = (3(x-1) + 2y)/\sqrt{13}$, and

$$y(x,y) = \begin{cases} f_1(s(x,y) + 1/2) & \text{for } s(x,y) \geqslant 0, \\ f_2(s(x,y) + 1/2) & \text{for } s(x,y) \leqslant 0, \end{cases}$$

for $f_1(s + 1/2) = -3s^5/128 - s^3/3$, $f_2(s + 1/2) = s^3/24 + s$, and $y_D = y|_{\partial\Omega}$. Then y is the unique solution of the convexification of 3.1 and the unique weak limit of any infimizing sequence for 3.1.

Fig. 3 displays the numerical solution on $\mathscr{T}_{10}$ generated by Algorithm 1. The adaptive strategy refines a region in which the exact solution has a discontinuity in the gradient. Fig. 4 shows various errors and the error estimator η_M for uniform and adaptive mesh refinement. We observe that the adaptive refinement strategy leads to significantly reduced errors and improved experimental convergence rates.

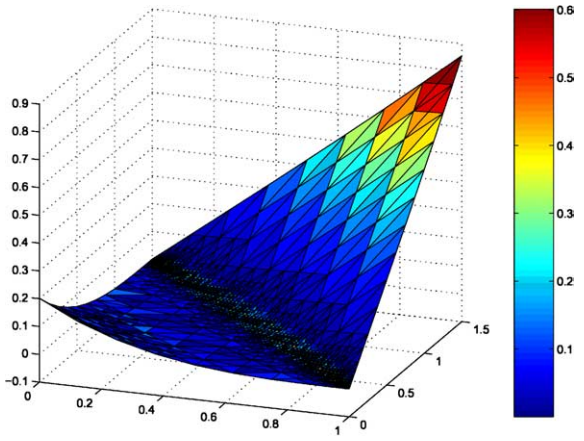

Fig. 3. Numerical solution y_h and modulus of the stress field $|DW^{**}(\nabla y_h)|$ (in gray shading) on the adaptively refined triangulation $\mathscr{T}_{10}$ in the scalar 2-well problem defined in Example 3.5. The adaptive strategy refines the mesh toward a line along which the gradient of the exact solution has a discontinuity.

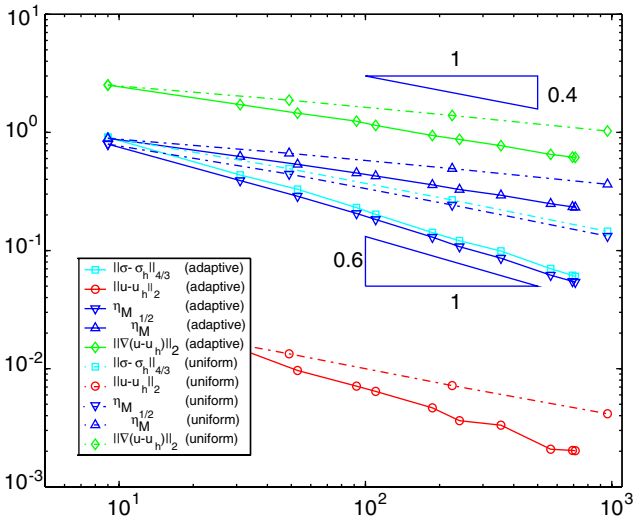

Fig. 4. Experimental convergence rates and error estimators η_M and $\eta_M^{1/2}$ plotted against degrees of freedom N with a logarithmic scaling for uniform and adaptive mesh refinement in the scalar 2-well problem defined in Example 3.5. The efficient estimator η_M serves as a good approximate of the stress error $\|\boldsymbol{\sigma} - \boldsymbol{\sigma}_h\|_{L^{4/3}(\Omega)}$. The reliable error estimator $\eta_M^{1/2}$ shows significantly slower convergence behavior. Adaptive mesh refinement improves the experimental convergence rate of $\|\boldsymbol{\sigma} - \boldsymbol{\sigma}_h\|_{L^{4/3}(\Omega)} \propto h^{0.6}$ to $\|\boldsymbol{\sigma} - \boldsymbol{\sigma}_h\|_{L^{4/3}(\Omega)} \propto h^{1.2}$.

3.6. Conclusions and open problems

The a posteriori error control suffers from the reliability-efficiency gap: The predicted upper and lower-error bounds (valid up to multiplicative constants and higher-order terms) are supported by the numerical results. The two bounds, however, converge with different rates and so leave an open scissor in Fig. 3 in the sense that the domain for the true error (i.e. the region between the lower and upper bound) becomes larger with smaller mesh-sizes. It remains as an open question whether and how this might be improved.

A numerical observation from [16] is supported for stabilized calculations as well: The averaging error estimator [12] is a very accurate error guess for the true stress error.

The strong convergence of the discrete solutions of the stabilized discrete problem is established in [39,7] for smooth solutions and (quasi-) uniform meshes. It is an open question whether and how to generalize those results to singular solutions on highly graded (unstructured) meshes. Additional regularity holds for the stress [19].

A numerical method with guaranteed convergence will be presented in the subsequent section. The result, however, is derived exclusively for convex minimization problems.

4. Convergence of quasi-Newton iteration

This section is devoted to the effective solution of the discrete relaxed problem utilizing a Newton– Raphson scheme with stabilization. The main result is global convergence for a stabilized quasi-Newton iteration first presented in an abstract framework and then applied to a discrete convexified minimization problem.

4.1. Abstract framework

To keep notation as general as possible we start with an abstract description and analysis of the quasi-Newton iteration.

Let V be a Hilbert space with induced norm $\|\cdot\|$ and with a family of scalar products $a_j : \times V \to \mathbb{R}$, $j = 1,2,3,\ldots$, which define equivalent norms $\|\cdot\|_{a_j}$ in the sense that there exist positive constants α_j and M_j such that

$$\alpha_j\|v\|^2 \leqslant a_j(v,v) \quad \text{and} \tag{4.1}$$

$$a_j(u,v) \leqslant M_j\|u\|\,\|v\| \quad \text{for all } u,v \in V. \tag{4.2}$$

Suppose $\varphi : V \to \mathbb{R}$ is $C1$ and uniformly convex and its derivative $D\varphi$ is Lipschitz in the sense that there exists positive constants α and L such that

$$\alpha\|u-v\|^2 + D\varphi(u;v-u) \leqslant \varphi(v) - \varphi(u) \quad \text{and} \tag{4.3}$$

$$(D\varphi(u) - D\varphi(v))(u-v) \leqslant L\|u-v\|^2 \quad \text{for all } u,v \in V. \tag{4.4}$$

Given an initial deformation $u_0 \in V$, the *quasi-Newton–Raphson scheme* defines a sequence $(u_j)_j$ in V recursively through

$$a_j(u_j - u_{j+1}, \cdot) = D\varphi(u_j) \quad \text{for } j = 0,1,2,\ldots \tag{4.5}$$

Theorem 4.1. Suppose that u_0 and u are arbitrary in V such that 4.5 defines a sequence $(u_j)_j$ and so defines $\delta_j := \varphi(u_j) - \varphi(u)$. Suppose that one iteration index j satisfies $0 \leqslant \delta_j$, δ_{j+1} and $0 < \alpha + \alpha_j - L$. Then there holds

$$\delta_{j+1} \leqslant (1 - 4\alpha(\alpha+\alpha_j-L)M_j^{-2})\delta_j \quad \text{and} \quad \|u-u_j\|^2 \leqslant M_j^2\alpha^{-2}(\alpha+\alpha_j-L)^{-1}(\delta_j - \delta_{j+1}).$$

Remark 4.1. The side restriction $L - \alpha < \alpha_0 \leqslant \alpha_j$ for some uniform α_0 and all j indicates a small damping parameter in a quasi-Newton–Raphson scheme.

Remark 4.2. Assuming $L - \alpha < \alpha_j$ for all j, the minimizer u of φ in V satisfies $\delta_j \geqslant 0$ and the theorem guarantees $\lim_{j\to\infty}\delta_j = 0$ and $\lim_{j\to\infty}\|u-u_j\| = 0$.

Remark 4.3. At first glance it may irritate in the theorem that u is *not* supposed to be the solution of $D\varphi(u) = 0$. In fact, the theorem provides some stability of the solution u as well: Any $u \in V$ with $\varphi(u) \leqslant \varphi(u_j)$, $\varphi(u_{j+1})$ satisfies $\|u - u_j\|^2 \leqslant M_j^2 \alpha^{-2}(\alpha + \alpha_j - L)^{-1}(\varphi(u_j) - \varphi(u_{j+1}))$.

4.2. Proof of theorem 4.1

With (4.3) and $\varphi(u) \leqslant \varphi(u_j), \varphi(u_{j+1})$ there holds

$$\alpha\|u - u_j\|^2 - D\varphi(u_j; u - u_j) \leqslant \varphi(u) - \varphi(u_j) = -\delta_j.$$

This and (4.5) followed by (4.2) and Young's inequality show

$$\begin{aligned}\alpha\|u - u_j\|^2 + \delta_j &\leqslant D\varphi(u_j; u_j - u) = a_j(u_j - u_{j+1}, u_j - u) \leqslant M_j\|u - u_j\|\|u_j - u_{j+1}\| \\ &\leqslant M_j^2/(4\alpha)\|u_j - u_{j+1}\|^2 + \alpha\|u - u_j\|^2,\end{aligned}$$

whence

$$\delta_j \leqslant \left(M_j^2/(4\alpha)\right)\|u_{j+1} - u_j\|^2. \tag{4.6}$$

A similar argument with (4.3) yields

$$\alpha\|u_{j+1} - u_j\|^2 + D\varphi(u_{j+1}; u_j - u_{j+1}) \leqslant \varphi(u_j) - \varphi(u_{j+1}) = \delta_j - \delta_{j+1}.$$

This and (4.4) and (4.5) followed by (4.1) leads to

$$\begin{aligned}\delta_{j+1} - \delta_j + \alpha\|u_{j+1} - u_j\|^2 &\leqslant (D\varphi(u_j) - D\varphi(u_{j+1}))(u_j - u_{j+1}) + D\varphi(u_j; u_{j+1} - u_j) \\ &\leqslant L\|u_{j+1} - u_j\|^2 - a_j(u_{j+1} - u_j, u_{j+1} - u_j) \\ &\leqslant (L - \alpha_j)\|u_{j+1} - u_j\|^2,\end{aligned}$$

whence

$$(\alpha + \alpha_j - L)\|u_{j+1} - u_j\|^2 \leqslant \delta_j - \delta_{j+1}. \tag{4.7}$$

The combination of (4.6) and (4.7) proves the first assertion. The second assertion follows from a modification of the aforementioned proof of (4.6) by utilizing (4.7) and Young's inequality:

$$\begin{aligned}\alpha\|u - u_j\|^2 + \delta_j &\leqslant M_j\|u - u_j\|\|u_j - u_{j+1}\| \leqslant \left[M_j/(\alpha + \alpha_j - L)^{1/2}\right]\|u - u_j\|(\delta_j - \delta_{j+1})^{1/2} \\ &\leqslant \alpha/2\|u - u_j\|^2 + M_j^2(\alpha + \alpha_j - L)^{-1}/(2\alpha)(\delta_j - \delta_{j+1}). \qquad \square\end{aligned}$$

4.3. Application

The following algorithm realizes the quasi-Newton–Raphson scheme and aims to minimize a functional $\varphi : \mathscr{A}_h \to \mathbb{R}$, where for simplicity we assume that $\mathscr{A}_h$ involves Dirichlet boundary conditions on the whole boundary $\partial\Omega$. We suppose that φ satisfies the assumptions of Theorem 4.1 with $V = \mathscr{S}_0^1(\mathscr{T})$ and the norm $\|\cdot\|$ induced by the scalar product

$$(u, v) = \int_\Omega \nabla u \cdot \nabla v \, d\mathbf{x}$$

and define

$$a_j(u,v) = \alpha_j \int_\Omega \nabla u \cdot \nabla v \, \mathrm{d}\mathbf{x} \tag{4.8}$$

with a parameter α_j that satisfies $L - \alpha < \alpha_j$.

Algorithm 2 (Quasi-Newton–Raphson iteration). Input: tolerance TOL > 0, triangulation $\mathscr{T}$, initial value $y_0 \in \mathscr{A}_h$, $j := 0$.

(a) Compute α_j and solve for $y_j + 1 \in \mathscr{A}_h$:

$$\alpha_j(y_j - y_{j+1}, v) = D\varphi(y_j; v) \quad \text{for all } v \in \mathscr{S}^1_0(\mathscr{T}).$$

(b) Stop if $(\sum_{z\in\mathscr{K}} |\, D\varphi(y_{j+1}, \varphi_z)|^2)^{1/2} \leqslant \mathrm{TOL}$, where φ_z are the nodal basis functions associated to the free nodes $z \in \mathscr{K}$.

(c) Set $j = j + 1$ and go to (a).

If we replace $\alpha_j(y_j - y_{j+1}, v)$ by $D^2\varphi(y_j; y_j - y_{j+1}, v)$ in Step (a) of the preceding algorithm we recover the classical Newton–Raphson scheme.

Algorithm 3 (Classical Newton–Raphson iteration). Input: tolerance TOL > 0, triangulation $\mathscr{T}$, initial value $y_j \in \mathscr{A}_h$ for $j = 0$.

(a) Solve for $y_j + 1 \in \mathscr{A}_h$:

$$D^2(\varphi_j; y_j - y_{j+1}, v) = D\varphi(y_j; v) \quad \text{for all } v \in \mathscr{S}^1_0(\mathscr{T}).$$

(b) Stop if $\left(\sum_{z\in\mathscr{K}} |\, D\varphi(y_{j+1}, \varphi_z)|^2\right)^{1/2} \leqslant \mathrm{TOL}$.

(c) Set $j = j + 1$ and go to (a).

4.4. Numerical experiment

Theorem 4.1 proves convergence for the quasi Newton–Raphson scheme to the minimizer of φ under general assumptions, i.e. uniform convexity of φ and uniform Lipschitz continuity of $D\varphi$ as well as an appropriate choice of the parameters α_j. In the stabilized scalar 2-well problem 3.3, where

$$\varphi(y) = \int_\Omega W^{**}(\nabla y)\mathrm{d}\mathbf{x} + \|y - \overline{y}\|^2_{L2(\Omega)} + h\|\nabla y\|^2_{L2(\Omega)} - \int_\Omega fy \, \mathrm{d}\mathbf{x},$$

assumption 4.3 is satisfied with $\alpha = h$. Uniform Lipschitz continuity 4.4 of $D\varphi$ does not hold in this example but φ is continuously differentiable and Lipschitz continuous on every bounded subset of $\mathscr{A}_h$. We employed

$$\alpha_j = 50$$

in 4.8. The parameter α in 4.1 is proportional to the (small) mesh-size h so that the error after the jth iteration is $\|\nabla(y - y_j)\|^2_{L2(\Omega)} \leqslant Ch^{-2}\theta^j$ where y is the minimizer of $\varphi = E^{**}_h$ in $\mathscr{A}_h$ and $\theta \in (0,1)$. The functional φ is uniformly convex but not twice continuously differentiable so that (quadratic) convergence of classical Newton–Raphson schemes is unclear. The following numerical comparison shows however that nested Newton–Raphson schemes are most efficient in the case of Example 3.3.

Table 1 displays the number of iterations needed to achieve a residual less than 3% of the initial residual on the respective triangulation, i.e. we chose

Table 1
Iteration numbers for the (nested) quasi-Newton–Raphson and the (nested) classical Newton–Raphson scheme in the stabilized 2-well problem 3.3 for different mesh-sizes and uniform meshes

h	Quasi-Newton–Raphson	Classical Newton–Raphson
1/4	4	2
1/8	4	2
1/16	5	2
1/32	6	2

The number of iteration steps remains bounded for the classical Newton–Raphson scheme and grows slowly in the quasi-Newton–Raphson scheme.

$$\mathrm{TOL} := 0.3\left(\sum_{z\in\mathcal{K}} |D\varphi(y_{j+1},\varphi_z)|^2\right)^{1/2}$$

in Algorithms 2 and 3.

We used uniform meshes with mesh-sizes $h = 1/4, 1/8, 1/16, 1/32$ and we employed a nested iteration technique which means that given an approximate solution Y on a mesh $\mathcal{T}_k$ the starting value y_0 for the iteration in Algorithms 2 and 3 on a finer mesh $\mathcal{T}_{k+1}$ was obtained from a linear prolongation of Y onto $\mathcal{T}_{k+1}$.

5. Elastic 2-well problem

This section is devoted to the numerical approximation of a two-dimensional model which is motivated by the mathematical description of phase transitions for crystalline solids, namely for the high-temperature super-conducting $TB_2Cu_3O_{6+x}$ material which undergoes an austenite-to-martensite phase-change.

5.1. Non-convex energy density and its quasiconvexification

We model the phase-transition in two dimensions as being cubic-to-tetragonal, which constitutes a simplification compared to the behavior of the actual material. The non-convex minimization problem then involves eigenstrains

$$\mathbf{E}_1 = -0.0113\mathbf{m}\otimes\mathbf{m} - 0.0102\mathbf{n}\otimes\mathbf{n} \qquad \text{and} \qquad \mathbf{E}_2 = -0.0102\mathbf{m}\otimes\mathbf{m} - 0.0113\mathbf{n}\otimes\mathbf{n}$$

for $\mathbf{m} = (\cos(\pi/3), \sin(\pi/3))$ and $\mathbf{n} = (-\sin(\pi/3), \cos(\pi/3))$, and the material tensor $\mathbb{C}$ defined for cubic anisotropy by

$$\mathbb{C}\mathbf{E} = \lambda\mathrm{tr}(\mathbf{E})\mathbf{Id} + 2\mu\mathbf{E} + \alpha(\mathbf{n}\otimes(\mathbf{E}\mathbf{n}) + (\mathbf{E}\mathbf{n})\otimes\mathbf{n})$$

with material parameters $\lambda = -67$, $\mu = 137$, and $\alpha = 40$. In a geometrically linearized setting, the energy density W is modeled as the infimum of two elastic energies

$$W_j(\mathbf{E}) = \tfrac{1}{2}\mathbb{C}(\mathbf{E}-\mathbf{E}_j) : (\mathbf{E}-\mathbf{E}_j) \quad \text{for } j = 1, 2,$$

corresponding to the two energy minima $\mathbf{E}_1, \mathbf{E}_2 \in \mathbb{R}_n \times n$ and with the scalar product $\mathbf{A}:\mathbf{B}$ in $\mathbb{R}^n \times n$,

$$W(\mathbf{E}) := \min\{W_1(\mathbf{E}), W_2(\mathbf{E})\}.$$

The quasiconvex envelope is explicitly known [31]

$$W^{\mathrm{qc}}(\mathbf{E}) = \begin{cases} W_1(\mathbf{E}) & \text{for } W_2(\mathbf{E}) + \alpha \leqslant W_1(\mathbf{E}), \\ \frac{1}{2}(W_2(\mathbf{E}) + W_1(\mathbf{E})) - \frac{1}{4\gamma}(W_2(\mathbf{E}) - W_1(\mathbf{E}))^2 - \frac{4}{\alpha} & \text{for } |W_1(\mathbf{E}) - W_2(\mathbf{E})| \leqslant \alpha, \\ W_2(\mathbf{E}) & \text{for } W_1(\mathbf{E}) + \alpha \leqslant W_2(\mathbf{E}) \end{cases}$$

for some $\alpha > 0$ defined in terms of $\mathbb{C}$, $\mathbf{E}_1$, and $\mathbf{E}_2$. The aforementioned Green strains $\mathbf{E}_1$ and $\mathbf{E}_2$ are compatible in the sense that

$$\mathbf{E}_1 - \mathbf{E}_2 = (\mathbf{a} \otimes \mathbf{b} + \mathbf{b} \otimes \mathbf{a})/2 \quad \text{holds for some } \mathbf{a}, \mathbf{b} \in \mathbb{R}^n.$$

Then, $\alpha = \frac{1}{2}(\mathbf{E}_1 - \mathbf{E}_2) : \mathbb{C}(\mathbf{E}_1 - \mathbf{E}_2)$ and the quasiconvex hull is convex: $W^{\mathrm{qc}} = W^{**}$.
It is stressed that this might not be the case for other materials.

5.2. Relaxed minimization problem and its discretization

Given a displacement $\mathbf{y}$, the linear Green strain tensor is the symmetric part of the displacement gradient,

$$\boldsymbol{\varepsilon}(\mathbf{y}) = \big(D\mathbf{y} + (D\mathbf{y})^T\big)/2.$$

Then, given $\mathbf{f} \in L_2(\Omega; \mathbb{R}_2)$, $\mathbf{g} \in L_2(\Gamma_N; \mathbb{R}_2)$ where $\Omega := (0,1)^2$, $\Gamma_D = [0,1] \times \{0\}$, $\Gamma_N = \partial\Omega \backslash \Gamma_D$, and the admissible displacements

$$\mathscr{A} = \{\mathbf{v} \in W^{1,2}(\Omega; \mathbb{R}^2) : \mathbf{v}|_{\Gamma_D} = 0\},$$

the relaxed minimization problem reads:

$$\text{Minimize } E^{\mathrm{qc}}(\mathbf{y}) = \int_\Omega W^{\mathrm{qc}}(\boldsymbol{\varepsilon}(\mathbf{y}))\mathrm{d}\mathbf{x} + \int_\Omega \mathbf{f} \cdot \mathbf{y}\mathrm{d}\mathbf{x} + \int_{\Gamma_N} \mathbf{g} \cdot \mathbf{y}\mathrm{d}\mathbf{s} \text{ among } \mathbf{y} \in \mathscr{A}. \tag{5.1}$$

With the finite element approximation space

$$\mathscr{A}_h := \{\mathbf{v}_h \in \mathscr{S}^1(\mathscr{T})^2 : \mathbf{v}_h|_{\Gamma_D} = \mathbf{0}\},$$

the discrete problem reads:

$$\text{Minimize } E^{\mathrm{qc}}(\mathrm{u}_h) = \int_\Omega W^{\mathrm{qc}}(\boldsymbol{\varepsilon}(\mathbf{y}_h))\,\mathrm{d}\mathbf{x} + \int_\Omega \mathbf{f} \cdot \mathbf{y}\,\mathrm{d}\mathbf{x} + \int_{\Gamma_N} \mathbf{g} \cdot \mathbf{y}\mathrm{d}\mathbf{s} \text{ among } \mathbf{y}_h \in \mathscr{A}_h. \tag{5.2}$$

5.3. A priori and a posteriori error control

In the compatible case, it has been shown in [21] that the discrete stresses $\boldsymbol{\sigma}_h = DW^{**}(\varepsilon(\mathbf{y}_h))$ converge strongly in $L^2(\Omega; \mathbb{R}^{2\times 2})$ to the exact unique stress $\boldsymbol{\sigma} = DW^{**}(\varepsilon(\mathbf{y}))$ in L^2 for $h \to 0$,

$$\|\boldsymbol{\sigma}_h - \boldsymbol{\sigma}\|_{L^2(\Omega)} \leqslant C \inf_{\mathbf{v}_h \in \mathscr{A}_h} \|\mathbf{y} - \mathbf{v}_h\|_{L^2(\Omega)}.$$

Moreover, a posteriori error estimates similar to 3.3 can be established and used for adaptive mesh refinement

$$\eta_M := \left(\sum_{T \in \mathscr{T}} \eta_T^2\right)^{1/2} \quad \text{and} \quad \eta_T = \|\boldsymbol{\sigma}_h - \boldsymbol{\sigma}_h^*\|_{L^2(T)},$$

where $\boldsymbol{\sigma}_h^*$ minimizes $\|\boldsymbol{\sigma}_h - \boldsymbol{\tau}_h\|_{L^2(\Omega)}$ among $\boldsymbol{\tau}_h \in \mathscr{S}^1(\mathscr{T})^2$.
These refinement indicators lead to the same strategy as described in Algorithm 1.

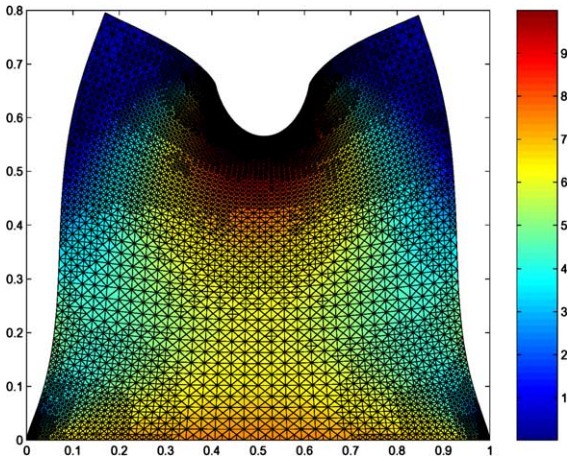

Fig. 5. Numerical solution $\mathbf{y}_h$ and modulus of the induced stress field for adaptive mesh refinement in Example 5.2. The deformation is amplified by a factor 10.

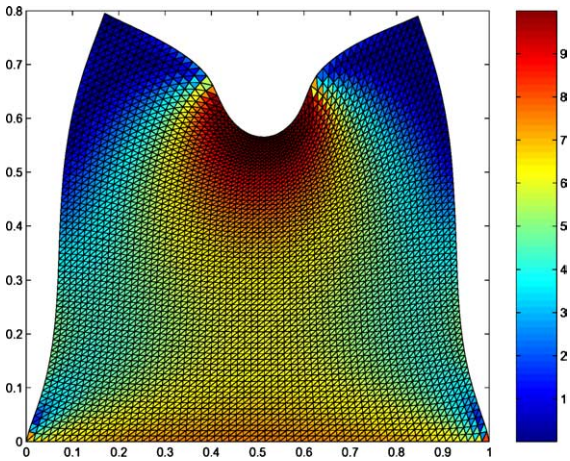

Fig. 6. Numerical solution $\mathbf{y}_h$ and modulus of the induced stress field for uniform mesh refinement in Example 5.2. The deformation is amplified by a factor 10.

5.4. Numerical experiment

We consider the following mechanical example: set $\mathbf{f} = 0$ and

$$\mathbf{g}(\mathbf{s}) = \begin{cases} (0,-10) & \text{for } \mathbf{s} \in [1/4, 3/4] \times \{1\}, \\ (0,0) & \text{for } \mathbf{s} \in \Gamma_N \setminus ([1/4, 3/4] \times \{1\}). \end{cases}$$

Fig. 8 below illustrates the physical problem and Fig. 5 displays the numerical solution on $\mathscr{T}_{10}$ generated by Algorithm 1 for $\Theta = 1/2$. Fig. 6 shows the numerical solution on the uniformly refined mesh $\mathscr{T}_2$. Notice that owing to the anisotropy in $\mathbb{C}$ the solution is not symmetric though the loads and the boundary conditions are symmetric.

5.5. Conclusions

The relaxation of the mechanical problem described in this section leads to a convex minimization problem which can be approximated very efficiently. Nested Newton–Raphson schemes (without stabilization) perform very well in practice and adapted meshes lead to significantly reduced energies. We stress however, that in this example the (convex) relaxed energy admits a regular second derivative almost everywhere in $\mathbb{R}^{2\times 2}$ which is not the case in general and then stabilization is a must. Moreover, the remarks on the reliability-efficiency gap and the open question of a more effective solution algorithm from Section 3.6 apply here as well. More difficult open problems include the efficient numerical treatment of 5.2 in case of incompatible zero strains, in which case there holds $W^{**} \neq W^{\mathrm{qc}}$.

6. Numerical approximation of effective energy densities

For all problems we considered so far the quasiconvex envelope W^{qc} has been available in analytical form. For most practical problems, however, this will not be the case and one has to resort to numerical approximations. But a direct approximation of W^{qc} is still very hard to do because its definition involves minimization over a large class of functions. More suitable for numerical schemes are either the polyconvex or the rank-1-convex envelope.

6.1. Numerical polyconvexification

The polyconvex envelope W^{pc} of the energy density function $W : \mathbb{R}^{m\times n} \to \mathbb{R}$ is given by the formula

$$W^{\mathrm{pc}}(\mathbf{F}) = \min\left\{\sum_{j=1}^{T_d+1}\lambda_j W(\mathbf{F}_j) : \lambda_j \geqslant 0, \mathbf{F}_j \in \mathbb{R}^{d\times d}, \sum_{j=1}^{T_d+1}\lambda_j = 1, \sum_{j=1}^{T_d+1}\lambda_j \operatorname{Minors}(\mathbf{F}_j) = \operatorname{Minors}(\mathbf{F})\right\}.$$

Here $\operatorname{Minors}(\mathbf{F})$ denotes the set of all Minors of $\mathbf{F}$, i.e $\operatorname{Minors}(\mathbf{F}) = (\mathbf{F}, \det\mathbf{F})$ for $n = 2$ and $\operatorname{Minors}(\mathbf{F}) = (\mathbf{F}, \operatorname{Cof}\mathbf{F}, \det\mathbf{F})$ for $n = 3$, and $T_n = \dim\operatorname{Minors}(\mathbf{F})$. The polyconvex envelope is polyconvex and hence quasiconvex as desired. In some situations, however, $W^{\mathrm{pc}}(\mathbf{F})$ and $W^{\mathrm{qc}}(\mathbf{F})$ can differ significantly.

The definition of $W^{\mathrm{pc}}(\mathbf{F})$ involves the solution of a global optimization problem, which may turn out to be difficult. It can be transformed into a linear optimization problem by the following approximation:

$$W^{\mathrm{pc}}_{d,r}(\mathbf{F}) = \min\left\{\sum_{\mathbf{A}\in\mathscr{N}_{d,r}}\lambda_{\mathbf{A}} W(\mathbf{A}) : \lambda_{\mathbf{A}} \geq 0, \sum_{\mathbf{A}\in\mathscr{N}_{d,r}}\lambda_{\mathbf{A}} = 1, \sum_{\mathbf{A}\in\mathscr{N}_{d,r}}\lambda_{\mathbf{A}} \operatorname{Minors}(\mathbf{A}) = \operatorname{Minors}(\mathbf{F})\right\}.$$

Here, for parameters $0 \leqslant d \leqslant r$ we define

$$\mathscr{N}_{d,r} := \{\mathbf{A} \in \mathbb{R}^{n\times n} \cap d\mathbb{Z}^{n\times n} : \max_{j,k} |\, \mathbf{A}_{jk} \,| \leqslant r\}$$

where $\mathbb{Z}$ denotes the set of all integers. The direct calculation of $W^{\mathrm{pc}}_{d,r}(\mathbf{F})$ is however difficult as it involves a large number of degrees of freedom, approximately $(r/d)^{n^2}$. Employing optimality conditions, one may design multilevel schemes with adaptive grid refinement and coarsening that iteratively compute the minimum

(typically within less than a second of CPU-time for $n = 2$ and an accuracy of 10^{-4}). Moreover, the combination of the optimality conditions with growth conditions on W allows for an a posteriori estimate which indicates whether the "diameter" r is chosen large enough to lead to an accurate approximation of $W^{pc}(\mathbf{F})$. For details on the algorithm, error estimates, and related numerical experiments we refer to [8].

6.2. Finite lamination

The *relaxation with respect to first-order laminates* of an energy density W reads (where frequently and without loss of generality $|\mathbf{b}| = 1$ is assumed)

$$R_1 W(\mathbf{F}) = \min_{0\leqslant\lambda\leqslant 1\mathbf{a},\mathbf{b}\in\mathbb{R}^n} \left\{ (1-\lambda) W(\underbrace{\mathbf{F} - \lambda \mathbf{a}\otimes\mathbf{b}}_{\mathbf{F}_1}) + \lambda W(\underbrace{\mathbf{F} + (1-\lambda)\mathbf{a}\otimes\mathbf{b}}_{\mathbf{F}_2}) \right\}. \tag{6.1}$$

The vectors $\mathbf{a}$ and $\mathbf{b}$ form the rank-one matrix $\mathbf{a}\otimes\mathbf{b}$ and the scalar λ describes the volume fraction of the two phases with deformation gradients $\mathbf{F}_1$ and $\mathbf{F}_2$, respectively. This means that we minimize with respect to all microstructure patterns as depicted in Fig. 2. Thus obviously, if W is rank-one-convex we have $R_1 W = W$.

It is well established that, in general $R_1 W$ is *not* rank-one-convex [47]. The situation improves by iterating the procedure, $R_1 R_1 W$ for example denoting the envelope with respect to second-order laminates. The limit $R_1 W = \lim_{\ell\to\infty} R_1^\ell W$ is the *rank-one-convex envelope*. Although $R_1 W$ is still not quasiconvex it is rank-one-convex or elliptic, i.e. satisfies the Cauchy–Hadamard-conditions. For many cases $R_1 W$ yields a close approximation to W^{qc}, see [33,45,28].

The relaxations $R_1^\ell W$ offer instructive information concerning the underlying microstructure, which we are going to describe now in detail. Following [24,45,25] we consider sets of pairs $\{\lambda_j,\mathbf{F}_j\}$, $j = 1,\ldots,N$, $2 \leqslant N \leqslant 2^\ell$ of probabilities λ_j and deformation gradients $\mathbf{F}_j$, with N accounting for the number of different gradients present.

Definition 6.1 (rank-one connectivity, $\mathscr{H}_N$). The pairs $\{\lambda_j,\mathbf{F}_j\}$ are called *rank-one connected* (written $\{\lambda_j,\mathbf{F}_j\} \in \mathscr{H}_N$) if $\lambda_j \geqslant 0$, $\sum_{j=1}^N \lambda_j = 1$ and the following holds.

(i) if $N = 2$, then rank $(\mathbf{F}_2 - \mathbf{F}_1) \leqslant 1$;
(ii) if $N > 2$, then, up to a permutation, rank $(\mathbf{F}_2 - \mathbf{F}_1) \leqslant 1$ and if

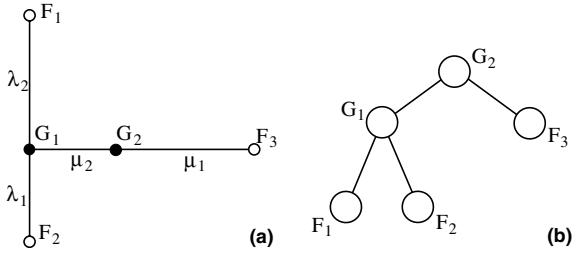

Fig. 7. Representations of rank-one connected deformation gradients $\{\lambda_j,\mathbf{F}_j\} \in \mathscr{H}_3$. The graph representation (a) consists of leaf nodes (deformation gradients $\mathbf{F}_j$) which are connected by edges (solid lines) representing rank-one families of matrices. The inner nodes ($\mathbf{G}_j$) are placed on the barycenter of the edges corresponding to the probabilities λ_j. (a) Graph representation (b) tree representation.

$$\mu_1 = \lambda_1 + \lambda_2, \qquad \mathbf{G}_1^{N-1} = \tfrac{1}{\lambda_1+\lambda_2}(\lambda_1\mathbf{F}_1 + \lambda_2\mathbf{F}_2),$$
$$\mu_j = \lambda_{j+1}, \qquad \mathbf{G}_j^{N-1} = \mathbf{F}_{j+1}, \quad j = 2, \ldots, N-1,$$

then $(\mu_j, \mathbf{G}_j^{N-1}) \in \mathscr{H}_{N-1}$.

The geometric interpretation of the definition above is given by a graph $\mathscr{G}(\lambda_j, \mathbf{F}_j)$ with leaves $\mathbf{F}_j$, inner nodes $\mathbf{G}_j$ and edges that are rank-one lines as in Fig. 7(a). For computational purposes the graph is often represented as a binary tree as in Fig. 7(b).

The relaxation $\mathrm{R}_1^\ell W$ is now given by

$$\mathrm{R}_1^\ell W(\mathbf{F}) = \min\left\{\sum_{j=1}^N \lambda_j W(\mathbf{F}_j) : \quad N \leqslant 2^\ell, \quad (\lambda_j, \mathbf{F}_j) \in \mathscr{H}_N, \quad \mathbf{F} = \sum_{j=1}^N \lambda_j \mathbf{F}_j\right\}. \tag{6.2}$$

We refer to Subsection 9.7 for a numerical comparison of these notions of convexity.

7. Numerical approximation of the polyconvexification of an energy density

There exists no general technique to find a closed formula for the quasiconvex envelope of a given energy density. The direct approximation is of the form discussed in Section 2 and hence extremely difficult. Instead of an inaccurate approximation of W^{qc} this section addresses the accurate approximation of the polyconvex envelope W^{pc} of the energy density function $W : \mathbb{R}^n \times n \to \mathbb{R}$ described in Section 6.1 which leads to a lower bound of W^{qc}. The approximate polyconvex envelope can be employed for effective simulations:

$$\text{Minimize } E_d^{\mathrm{pc}}(\mathbf{y}_h) = \int_\Omega W_d^{\mathrm{pc}}(D\mathbf{y}_h)\,\mathrm{d}\mathbf{x} + \int_\Omega \mathbf{f}\cdot\mathbf{y}_h\,\mathrm{d}x + \int_{\Gamma_N} \mathbf{g}\cdot\mathbf{y}_h\,\mathrm{d}\mathbf{s} \text{ among } \mathbf{y}_h \in \mathscr{A}_h. \tag{7.1}$$

Error estimates can only be expected for the convergence of the energies, i.e. for $|\min_{\mathbf{v}\in\mathscr{A}} E^{\mathrm{pc}}(\mathbf{v}) - \min_{\mathbf{v}_h\in\mathscr{A}_h} E_d^{\mathrm{pc}}(\mathbf{v}_h)|$, but require additional regularity of the exact solution.

Since it would be inefficient to compute W_d^{pc} in the whole (or a large subset of) $\mathbb{R}^{2\times 2}$ we employ the following iterative algorithm which realizes a steepest descent method to approximate a local minimizer of E_d^{pc}.

Algorithm 4 (Outer loop in numerical polyconvexification). Input: initial $\mathbf{y}_h^{(0)} \in \mathscr{S}^1_D(\mathscr{T})^2$, tolerance $\delta > 0$, parameter $d > 0$, and $j := 0$.

(a) Run Algorithm 5 to compute $\boldsymbol{\sigma}_h := DW_d^{\mathrm{pc}}(D\mathbf{y}_h^{(j)})$.

(b) Let $\mathbf{r}_h \in \mathscr{S}^1_D(\mathscr{T})^2$ be such that, for all $\mathbf{v}_h \in \mathscr{S}^1_D(\mathscr{T})^2$,

$$\int_\Omega D\mathbf{r}_h : D\mathbf{v}_h\,\mathrm{d}\mathbf{x} = -\int_\Omega \boldsymbol{\sigma}_h\cdot\nabla\mathbf{v}_h\,\mathrm{d}\mathbf{x} - \int_\Omega \mathbf{f}\cdot\mathbf{v}_h\,\mathrm{d}\mathbf{x} - \int_{\Gamma_N}\mathbf{g}\cdot\mathbf{v}_h\,\mathrm{d}\mathbf{s}.$$

(c) Compute an approximation t_δ^* of a local minimizer $t^* \in [0,1]$ of $e(t)$,

$$e(t) = \int_\Omega \tau_h(t)\,\mathrm{d}\mathbf{x} + \int_\Omega \mathbf{f}\cdot(\mathbf{y}_h^{(j)} + t\mathbf{r}_h)\,\mathrm{d}\mathbf{x} + \int_{\Gamma_N}\mathbf{g}\cdot(\mathbf{y}_h^{(j)} + t\mathbf{r}_h)\,\mathrm{d}\mathbf{s}.$$

Therein, Algorithm 5 is run to compute for given t, $\tau_h(t) = W_d^{\mathrm{pc}}\left(D(\mathbf{y}_h^{(j)} + t\mathbf{r}_h)\right)$.

(d) Stop if $t_\delta^* \leqslant \delta := 0.01$.

(e) Set $\mathbf{y}_h^{(j+1)} := \mathbf{y}_h^{(j)} + t_\delta^*\mathbf{r}_h$, $j := j+1$, and go to (a).

Output: an approximation of a local minimizer of $E_{d,h}^{\mathrm{pc}}$.

Remark 7.1. The numerical minimization of $e(t)$ in (c) was realized with a simple search routine which starts with $t_1 = 0$ and $t_4 = 1$:

(i) Choose t_2, t_3 such that $t_1 < t_2 < t_3 < t_4$ and compute $s_j = e(t_j)$.
(ii) If $s_3 \leqslant s_2$ set $t_1 = t_2$. Otherwise, set $t_4 = t_3$.
(iii) Stop if $t_4 - t_1 \leqslant \delta$ and go to (i) otherwise.

A good choice of the values t_2 and t_3 in (c) may lead to very efficient numerical schemes.

The computation of W_d^{pc} and DW_d^{pc} is done in a loop over all finite elements and employs the following algorithm.

Algorithm 5 (Inner loop in numerical polyconvexification). Input: function $W : \mathbb{R}^{2\times 2} \to \mathbb{R}$, $\mathbf{F} \in \mathbb{R}^{2\times 2}$, parameters $d, r > 0$.

(a) Solve the linear optimization problem

$$\alpha := \min\left\{ \sum_{\mathbf{A}\in \mathrm{N}_{d,r}} \lambda_{\mathbf{A}} W(\mathbf{A}) : \lambda_{\mathbf{A}} \geqslant 0,\ \sum_{\mathbf{A}\in \mathrm{N}_{d,r}} \lambda_{\mathbf{A}} = 1,\ \sum_{\mathbf{A}\in \mathrm{N}_{d,r}} \lambda_{\mathbf{A}} \mathbf{T}(\mathbf{A}) = \mathbf{T}(\mathbf{F}) \right\},$$

where $\boldsymbol{T}(\mathbf{A}) = (\mathbf{A}, \det\mathbf{A})$ and $\mathrm{N}^{d,r} = \{\mathbf{A} \in \mathbb{R}^{2\times 2} \cap d\mathbb{Z}^{2\times 2} : \max_{j,k} \mid \mathbf{A}_{jk} \mid \leqslant r\}$. This gives α and a Lagrange multiplier $\boldsymbol{\lambda} \in \mathbb{R}^5$ for the constraint $\sum_{\mathbf{A}\in \mathrm{N}_{d,r}} \lambda_{\mathbf{A}} \mathbf{T}(\mathbf{A}) = \mathbf{T}(\mathbf{F})$. (The numerical solution of the linear optimization problem was realized in an adaptive multilevel scheme employing interior point solvers.)

(b) Check if r was large enough using optimality conditions and growth conditions of W (see [8] for details). Set $r := 2r$ and go to (a) if not and stop otherwise.

Output: $\tau := \alpha = W_d^{\mathrm{pc}}(\mathbf{F})$ and $\boldsymbol{\sigma} := \boldsymbol{\lambda} \cdot D\mathbf{T}(\mathbf{F}) = DW_d^{\mathrm{pc}}(\mathbf{F})$.

Remark 7.2. To avoid deformation gradients with negative determinant, the numerical experiments in Section 7.1 employed a nonlinear stabilization by adding

$$0.001 \int_\Omega \tilde{\log}(\det(\mathbf{1} + D(\mathbf{y}_h^{(j)} + t\mathbf{r}_h)))^2 \mathrm{d}\mathbf{x}$$

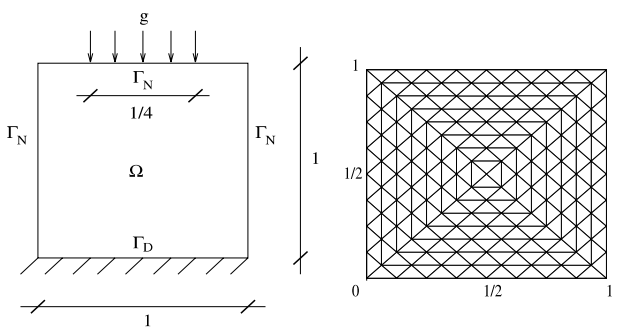

Fig. 8. Schematic description of the physical problem (left) and initial triangulation of Ω with 256 elements (right).

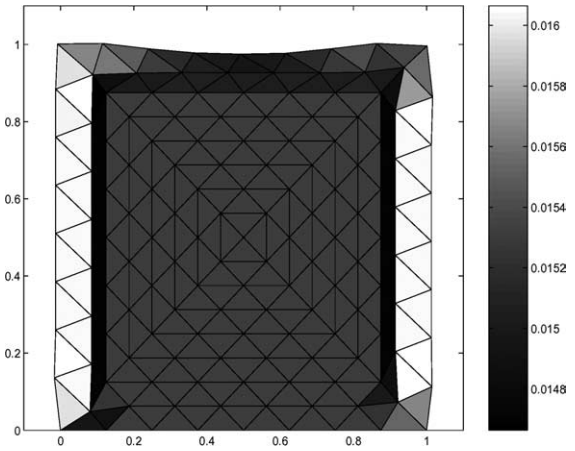

Fig. 9. Discrete deformation $\mathbf{y}_h$ of Ω (the displacement field is amplified by a factor 100 for illustrative purposes) together with the modulus of the induced discrete stress field $DW_d^{\mathrm{pc}}(D\mathbf{y}_h^{(6)})$.

where $\tilde{\log}(s) = \log(s)$ if $s > 0$ and $\tilde{\log}(s) := \infty$ if $s \leqslant 0$.

7.1. Numerical polyconvexification of a 2D Ericksen–James energy

Algorithm 4 ran for a 2D version of the Ericksen–James energy [40]. Here, given any deformation gradient $\mathbf{F} \in \mathbb{R}^{2\times 2}$ with Cauchy strain tensor $C = \begin{pmatrix} C_{11} & C_{12}, \\ C_{21} & C_{22} \end{pmatrix} := \mathbf{F}^T\mathbf{F}$, the frame-indifferent energy density reads

$$W(\mathbf{F}) := (\mathbf{C}_{11} + \mathbf{C}_{22} - 2)^2 + 0.3\mathbf{C}_{12}^2 + (\mathbf{C}_{11} - 1.1)^2(\mathbf{C}_{22} - 1.1)^2.$$

A phase transition is considered in a quadratic body $\Omega := (0,1)^2$ with homogeneous displacements along the Dirichlet boundary $\Gamma_D := [0,1] \times \{0\}$, no volume forces ($\mathbf{f} \equiv 0$, but loaded by a symmetric applied surface pressure $\mathbf{g} \in L^2(\Gamma_N)^2$ defined by $\mathbf{g}(s,1) = -(0,1/25)$ for $1/4 \ll s < 3/4$ along one half on top and $\mathbf{g} \equiv 0$ elsewhere as indicated in Fig. 8.

For a uniform triangulation of Ω with 256 elements shown in the right plot of Fig. 8, the initial choice $\mathbf{y}_h^{(0)} \equiv 0$, the algorithm terminated for $j = 6$. We thereby obtained the numerical approximation $\mathbf{y}_h = \mathbf{y}_h^{(6)} \in \mathscr{S}_D^1(\mathscr{T})^2$ of 7.1 displayed in Fig. 9 together with its induced discrete stress field $DW_d^{\mathrm{pc}}(Du_h)$. Quantitatively, the discrete deformation appears reasonable although we still assume a relatively large approximation error.

8. Time-evolution for inelastic materials

In this section we will discuss a variational setting for inelastic materials which allows to discuss the occurrence of microstructures in a rational way. We would like to do this in a finite-deformation setting.

8.1. Variational formulation

For inelastic materials the (specific Helmholtz free) energy $W(\mathbf{F},\mathbf{K})$ on the deformation gradient $\mathbf{F}=\nabla\mathbf{y}$ and on a set of internal variables $\mathbf{K}$. The latter measure the intrinsic state of the material produced by plastic deformation, hardening, damage or phase-transformations [35,36], cf. this work for more details.

In elasticity theory the deformation $\mathbf{y}$ constitutes the independent variable of the boundary value problem at hand and is determined via balance of momentum and appropriate boundary conditions. Now there is an additional set of independent variables $\mathbf{K}$ and we need an additional set of equations for our problem to be well-posed. Since the internal variables $\mathbf{K}$ describe the history of the material; their evolution equations are of the type (with $\dot{x}:=\mathrm{d}x/\mathrm{d}t$)

$$f(\mathbf{F},\dot{\mathbf{F}},\mathbf{K},\dot{\mathbf{K}})=0. \tag{8.1}$$

Any inelastic material is characterized by dissipation, which is non-recoverable energy expended via change of the internal variables, as described by the rate $\dot{\mathbf{K}}$. We capture this effect by introducing a *dissipation–functional* $\Delta(\mathbf{K},\dot{\mathbf{K}})$. As shown in [35,36] the time-evolution of the material body Ω under consideration is now governed by the Lagrange-functional

$$L(t,\mathbf{y}(t),\mathbf{K}(t),\dot{\mathbf{K}}(t))=\int_\Omega\left[\frac{\mathrm{d}}{\mathrm{dt}}W(\nabla\mathbf{y},\mathbf{K})+\Delta(\mathbf{K},\dot{\mathbf{K}})\right]\mathrm{d}V-\frac{\mathrm{d}}{\mathrm{dt}}\ell(t,\mathbf{y}). \tag{8.2}$$

Here $\ell(t,\mathbf{y})$ is the potential of external forces. Moreover $\mathbf{y}$ has to satisfy boundary conditions

$$\mathbf{y}(t)=\mathbf{y}_0(t)\qquad\text{on}\qquad\Gamma_0\subset\partial\Omega. \tag{8.3}$$

Static equilibrium and boundary conditions as well as evolution–equations for $\mathbf{K}$ can now be obtained via the least-action principle

$$\begin{aligned}\{\mathbf{y}(s)\equiv\mathbf{y}(t),\mathbf{K}(s)\equiv\mathbf{K}(t)\}=\arg\min\Bigg\{\int_0^1 L(s,\mathbf{y}(s),\mathbf{K}(s),\dot{\mathbf{K}}(s))\,\mathrm{d}s:\ \ &\mathbf{y}(s),\mathbf{K}(s),\mathbf{y}(s)\\ &=\mathbf{y}_0(t)\ \text{on}\ \Gamma_0,\mathbf{y}(0)=\mathbf{y}(t),\mathbf{K}(0)=\mathbf{K}(t)\Bigg\}.\end{aligned} \tag{8.4}$$

This means the "constant" solutions (in s) $\{\mathbf{y}(s)\equiv\mathbf{y}(t),\ \mathbf{K}(s)\equiv\mathbf{K}(t)\}$ are minimizers of the action-integral above, or, otherwise stated, it is not possible to lower the sum of stored and dissipated energy by any (virtual) perturbation of the state $\{\mathbf{y}(t),\mathbf{K}(t)\}$. The principle (2) especially yields the evolution law

$$\mathbf{Q}\in\frac{\partial\Delta}{\partial\dot{\mathbf{K}}}, \tag{8.5}$$

which constitutes an implicit relation of the form 8.1 for $\dot{\mathbf{K}}$ (subdifferentials are required for example in the case of plasticity, see [15]). Here $\mathbf{Q}=-\frac{\partial W}{\partial\mathbf{K}}$ is the conjugate quantity to $\mathbf{K}$ and the differential inclusion accounts for law of inequality-type as encountered for example in plasticity.

8.2. Reduction to the elastic case

The advantage of the formulation above is, that in a time-incremental setting it reduces to a pure minimization problem which can be analyzed by variational calculus. To this end we introduce the *dissipation-distance*

$$D(\mathbf{K}_0, \mathbf{K}_1) = \inf \left\{ \int_0^1 \Delta(\mathbf{K}(s), \dot{\mathbf{K}}(s))\, \mathrm{d}s : \mathbf{K}(0) = \mathbf{K}_0, \mathbf{K}(1) = \mathbf{K}_1 \right\}, \tag{8.6}$$

which gives the energy dissipated if the internal variables are changed from a state $\mathbf{K}_0$ to $\mathbf{K}_1$. Note that the minimization performed in the definition of $D(\mathbf{K}_0, \mathbf{K}_1)$ follows from the principle (2).

Let us consider a finite time-increment $[t_0, t_1]$ and let the values of the internal variables $\mathbf{K}_0 = \mathbf{K}(t_0)$ be known at the beginning of the increment. Then with the notion given above we obtain deformation $\mathbf{y}_1 = \mathbf{y}(t_1)$ and internal variables $\mathbf{K}_1 = \mathbf{K}(t_1)$ at the end of the increment from the following minimum-principle:

$$\{\mathbf{y}_1, \mathbf{K}_1\} = \arg\min \left\{ \int_\Omega \{W(\nabla \mathbf{y}, \mathbf{K}) + D(\mathbf{K}_0, \mathbf{K})\} \mathrm{d}V - \ell(t_1, \mathbf{y}) : \mathbf{y}, \mathbf{K}, \mathbf{y} = \mathbf{y}_0(t_1) \text{ on } \Gamma_0 \right\}. \tag{8.7}$$

This principle gives the exact equilibrium and boundary conditions at the end of the increment as well as an approximation of the evolution-equation for $\mathbf{K}$ depending on the size of the increment. Minimization over $\mathbf{K}$ can now be performed independently giving a *reduced potential*

$$W^{\mathrm{red}}_{\mathbf{K}_0}(\mathbf{F}) = \min \{W(\mathbf{F}, \mathbf{K}) + D(\mathbf{K}_0, \mathbf{K}) : \mathbf{K}\}, \tag{8.8}$$

along with the update formula

$$\mathbf{K}_1 = \arg\min \{W(\mathbf{F}, \mathbf{K}) + D(\mathbf{K}_0, \mathbf{K}) : \mathbf{K}\}. \tag{8.9}$$

This reduced potential, however, depends on $\mathbf{K}_0$ only as a parameter and can otherwise considered to be a purely elastic energy. We obtain the usual principle of minimum of energy:

$$\mathbf{y}_1 = \arg\min \left\{ \int_\Omega W^{\mathrm{red}}_{\mathbf{K}_0}(\nabla \mathbf{y}) \mathrm{d}V - \ell(t_1, \mathbf{y}) : \mathbf{y}, \mathbf{y} = \mathbf{y}_0(t_1) \text{ on } \Gamma_0 \right\}. \tag{8.10}$$

Thus any inelastic problem can be decomposed into a sequence of elastic by solving (8.10), updating $\mathbf{K}$ via (8.9) and continuing with the next time-increment.

For many inelastic materials $W(\mathbf{F},\mathbf{K})$ is taken to be quasiconvex in $\mathbf{F}$ whereas $\Delta(\mathbf{K}, \dot{\mathbf{K}})$ is even convex in $\dot{\mathbf{K}}$. Still $W^{\mathrm{red}}_{\mathbf{K}_0}(\mathbf{F})$ very often turns out not to be quasiconvex, leading to the evolution of microstructures as for example explained in [15]. Within a single time-increment we are now able to apply all the methods developed before to the reduced potential $W^{\mathrm{red}}_{\mathbf{K}_0}(\mathbf{F})$.

9. An application to single-slip elastoplasticity

In this section we will closely investigate a model of finite-strain elastoplasticity with a single slip-system which was introduced in [15] and proving to lead to a non-quasiconvex reduced potential.

9.1. Constitutive model and reduced potential

We start with assuming the well-established multiplicative split of the deformation gradient into an elastic and a plastic part: $\mathbf{F} = \mathbf{F_e}\mathbf{F_p}$. The set of internal variables $\mathbf{K} = \{\gamma, p\}$ consists of the scalar plastic slip γ and a hardening variable p. The plastic deformation $\mathbf{F_p}$ is entirely determined by γ, i.e.

$$\mathbf{F_p} = \mathbf{I} + \gamma \mathbf{s}_0 \otimes \mathbf{n}_0, \tag{9.1}$$

where $\boldsymbol{s}_0$ and $\boldsymbol{n}_0$ denote the referential tangent and normal vector to the slip plane, respectively. We choose a free energy density function of a compressible neo-Hookean type, which in accordance with plastic indifference depends on $\mathbf{F}$ only via $\mathbf{F}_e$:

$$W(\mathbf{F},\gamma,p) = U(j) + \frac{\mu}{2}\operatorname{tr}(\mathbf{F}_e^{\mathrm{T}}\mathbf{F}_e) + \frac{a}{2}p^2, \qquad U(j) = \frac{\Lambda}{4}(j)^2 - \frac{\Lambda+2\mu}{2}\ln(j),$$

in which the symbols μ, Λ and a denote material parameters. The set of forces conjugated to $\mathbf{K}$ is $\mathbf{T} = \{\tau,q\}$, with τ denoting the resolved shear stress. The yield function Φ and its corresponding characteristic function J read

$$\Phi(\tau,q) = \mid \tau \mid -r-q, \qquad J(\gamma,p,^{\mathrm{T}}\tau,q) = \begin{cases} 0 & \text{for } \Phi(\tau,q) \leqslant 0, \\ \infty & \text{else.} \end{cases} \tag{9.2}$$

By Legendre transform (for details we refer to [15]) we obtain the dissipation-function

$$\Delta(\gamma,p,\dot\gamma,\dot p) = \begin{cases} r \mid \dot\gamma \mid & \text{if } \mid \dot\gamma \mid +\dot p \leqslant 0, \\ \infty & \text{else} \end{cases} \tag{9.3}$$

for which the dissipation-distance D can be constructed explicitly as

$$D(\gamma_0,p_0,\gamma_1,p_1) = \begin{cases} r \mid \gamma_1-\gamma_0 \mid & \text{if } \mid \gamma_1-\gamma_0 \mid +p_1-p_0 \leqslant 0, \\ \infty & \text{else.} \end{cases} \tag{9.4}$$

Moreover, the minimization with respect to the internal variables can be carried out explicitly in this example and results in a closed expression for the reduced potential

$$W^{\mathrm{red}}_{\gamma_0,p_0}(\mathbf{F}) = U(\det\mathbf{F}) + \frac{\mu}{2}\left[\operatorname{tr}\mathbf{F}^{\mathrm{T}}\mathbf{F} - 2\gamma_0\ \mathbf{s}\cdot\mathbf{n} + \gamma_0^2\mathbf{s}\cdot\mathbf{s} - \frac{(\max\{0,\mid \mathbf{s}\cdot\mathbf{n} - \gamma_0\mathbf{s}\cdot\mathbf{s} \mid -\frac{\tau_{\mathrm{crit}}-ap_0}{\mu}\})^2}{\mathbf{s}\cdot\mathbf{s} + a/\mu}\right], \tag{9.5}$$

where $\mathbf{s} = \mathbf{F}\mathbf{s}_0$ and $\mathbf{n} = \mathbf{F}\mathbf{n}_0$ are the slip-system vectors in the deformed configuration. Energy density functions in finite elasticity and will be analyzed for its convexity properties.

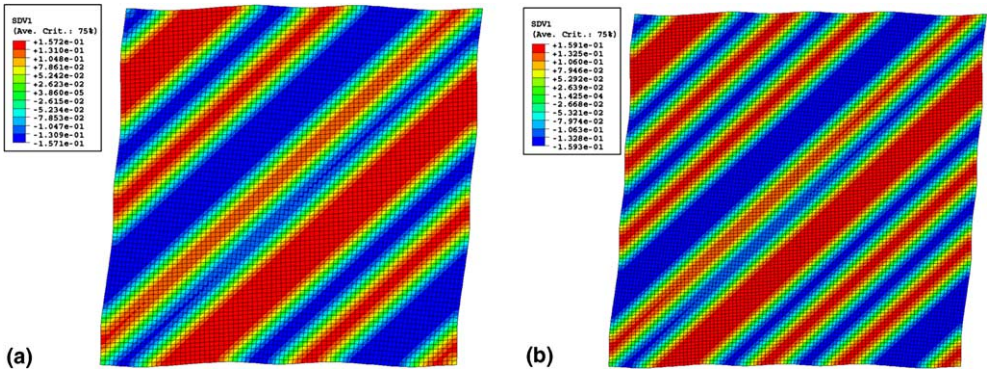

Fig. 10. FE simulation, contour: plastic slip γ, deformation = $F_{12} = 0.1$, results are mesh-dependent but effective properties, for example volume ratios, are not. (a) 6400 elements, (b) 10,000 elements.

9.2. Direct finite element simulation

The occurrence of microstructures can be demonstrated by finite element analysis. We consider a plane shear deformation of a representative volume element (RVE) consisting of standard 4-node plane strain elements subjected to periodic boundary conditions. The RVE models the micro-scale behavior of a single material point for a given macro-deformation **F**. The material parameters ($\Lambda = 15000$ MPa, $\mu = 10000$ MPa, $\tau_{\text{crit}} = 10$ MPa, $\phi = -45.0°$, $a = 1000$ MPa) are chosen to obtain significant microstructure formation.

The loss of quasiconvexity is a global phenomenon. Hence microstructures will already be possible as a global minimizer at a point where the potential is locally still elliptic and thus has the homogeneous solution as local minimizer. Therefore we have to stimulate the formation of microstructures. Two different methods have been applied for this purpose:

(A) *Static perturbation*: A randomly oriented field of distributed forces of a small magnitude is applied to the structure in order to perturb the initial stable state of the material. With an appropriate choice of the perturbation load, microstructures will form up and the initial perturbation load can be released. The macro deformation gradient **F** is kept fixed during the perturbation process, which forces the structure to accommodate solely by internal fluctuations.

(B) *Dynamic perturbation*: A randomly oriented velocity field is used to initiate internal fluctuations while the macro deformation gradient **F** is kept fixed. Then the magnitude of the velocity is reduced continuously by structural damping. With an appropriate choice of the intensity, orientation and damping of the velocity field the material will find a new rest state of lower energy and microstructures will show up.

Essentially, both methods lead to the same results. Fig. 10 shows contour plots of the plastic slip γ for FE simulations with different mesh sizes. The equilibrium state exhibits a laminar structure composed of opposite plastic slip. The number of oscillations (laminates) is mesh-depended. Macroscopic quantities like volume ratios or orientation of the laminates, however, are preserved for different meshes. Those are the quantities which enter into relaxation theory.

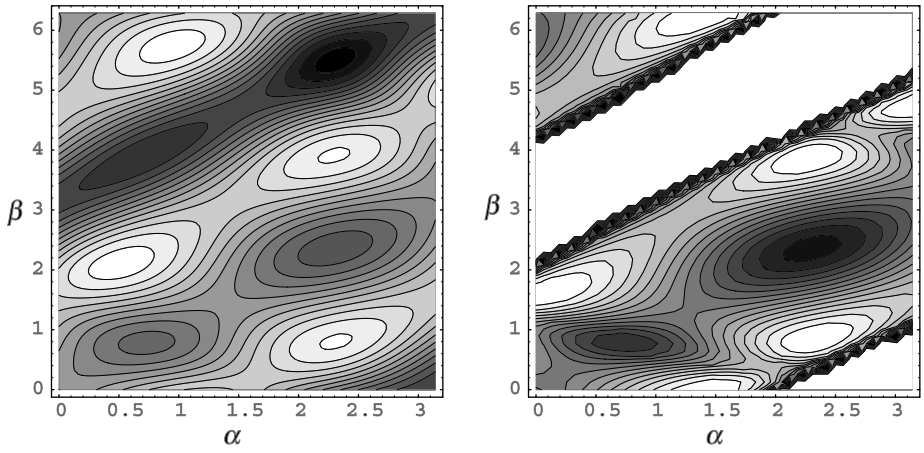

Fig. 11. Multiple minima (white) in contour plots of the objective function (9.6) projected on the α–β-plane. Parameters $\lambda = 0.1$, $\rho = 0.6$ (left) and $\rho = 2.1$ (right).

9.3. Finite lamination

We will calculate the relaxations $R_1 W^{\mathrm{red}}$ and $R_1^2 W^{\mathrm{red}}$ for the reduced potential as introduced in Section 6.2. The computation can be formulated as a restricted optimization problem. For the two-dimensional case and $n = 1$ the objective function

$$\widetilde{W}^{\mathrm{red}}(\mathbf{x}, \mathbf{F}) := (1-\lambda) W^{\mathrm{red}}(\underbrace{\mathbf{F} - \lambda \mathbf{a} \otimes \mathbf{b}}_{\mathbf{F}_1}) + \lambda W^{\mathrm{red}}(\underbrace{\mathbf{F} + (1-\lambda)\mathbf{a} \otimes \mathbf{b}}_{\mathbf{F}_2}) \tag{9.6}$$

depends on four optimization variables

$$\mathbf{x} = (\lambda, \rho, \alpha, \beta), \quad \mathbf{a} = \rho \begin{pmatrix} \cos(\alpha) \\ \sin(\alpha) \end{pmatrix}, \quad \mathbf{b} = \begin{pmatrix} \cos(\beta) \\ \sin(\beta) \end{pmatrix}. \tag{9.7}$$

The vectors $\mathbf{a}$ and $\mathbf{b}$ form the rank-one matrix $\mathbf{a} \otimes \mathbf{b}$ and the scalar λ describes the volume fraction of the two phases with deformation gradients $\mathbf{F}_1$ and $\mathbf{F}_2$, respectively. The relaxed energy is obtained by solving the minimization problem

$$R_1 W^{\mathrm{red}}(\mathbf{F}) = \min_{\mathbf{x} \in \mathscr{B}} \widetilde{W}^{\mathrm{red}}(\mathbf{x}, \mathbf{F}) \tag{9.8}$$

for a given $\boldsymbol{F}$, where the domain $\mathscr{B}$ of $\boldsymbol{x}$ is

$$\mathscr{B} = \{\mathbf{x} \in \mathbb{R}^4 \mid 0 \leqslant \lambda \leqslant 1, 0 \leqslant \rho, 0 \leqslant \alpha \leqslant \pi, 0 \leqslant \beta \leqslant 2\pi, \det(\mathbf{F}i) > 0\}. \tag{9.9}$$

9.4. Global minimization algorithms

The task of global optimization is to find a solution in the solution set $\mathscr{B}$ for which the objective function (9.6) obtains its smallest value, the global minimum. The contour plots Fig. 11 show that the objective function (9.6) has several local extrema and the domain $\mathscr{B}$ may be bounded non-simply, [43,49], because of the constraints $\det \mathbf{F}_i > 0$.

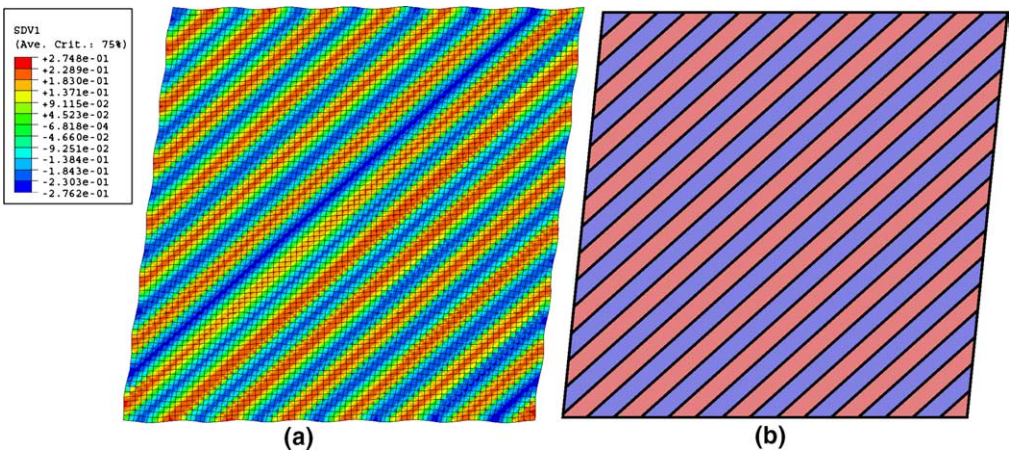

Fig. 12. First-order laminar microstructure, contour: plastic slip γ, macroscopic properties are recovered by relaxation method. (a) FE simulation using 6400 elements, (b) numerical relaxation using $R_1 W$.

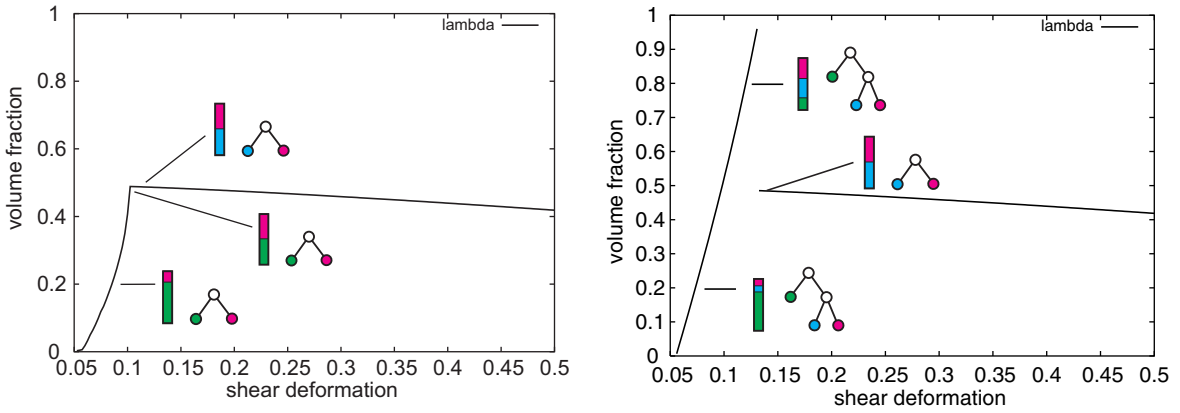

Fig. 13. Volume fractions λ, usage of second-order laminates gives significantly different results. (a) First-order laminate, (b) second-order laminate.

We have used different methods (e.g. branch and bound, clustering, interval, see [43]) to solve the optimization problem (9.8). Probabilistic global search procedures like multi-start and clustering algorithms have shown to be efficient and sufficiently robust. The basic idea of the family of multi-start methods is to apply a local search procedure several times and evaluate the function (9.6) at each of those points. A drawback of this method is that when many starting points are used the same local minimum may be identified several times. This leads to an inefficient global search. Clustering methods attempt to avoid this inefficiency by carefully selecting points at which the local search is initiated.

Algorithm 6 (Global optimization). Input: $\mathbf{F}$, initial population $\mathbf{x}_i \in \mathscr{B}$ of n points ($n \approx 100 \cdots 10{,}000$) in a feasible domain $\mathscr{B}$, tolerance $\delta > 0$.

(a) *Sampling and reduction*: Sample $\widetilde{W}^{\mathrm{red}}(x_i, F)$ for $\mathbf{x}_i \in \mathscr{B}$ and reduce the population by choosing the m best points.
(b) *Clustering*: Identify clusters, such that the points inside a cluster are "close" to each other, and the clusters are "far" from each other. If the clusters do not separate sufficiently, repeat step 1 with a bigger population in the whole domain or in specific regions.
(c) *Center of attraction*: Identify a center of attraction in each cluster: This could be the best point or the centroid of the subset of best points.
(d) *Local search*: Start a local search from the center of attraction, stop when minimum min is achieved with tolerance δ.

Output: $R_1^l(\mathbf{F}) = \min$.

Clustering algorithms are effective for low-dimensional problems, where the evaluation of the objective function is inexpensive. Constraints can be taken into account by removing sampling points which lie outside of the feasible domain. The final local search step is done by a quasi-Newton algorithm (unconstrained) or a sequential quadratic programming algorithm [46]. The latter was used to handle nonlinear constraints near the boundary of the feasible domain.

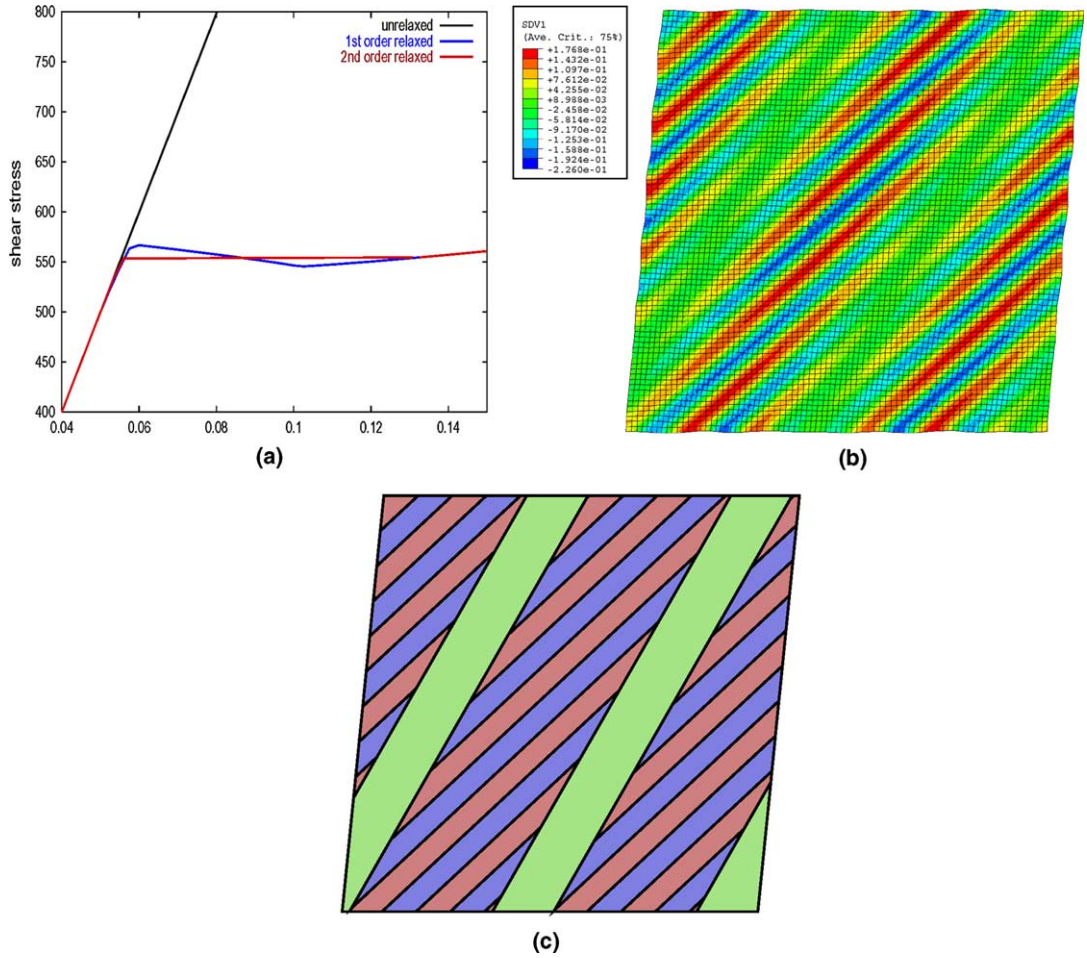

Fig. 14. Second-order laminar microstructure, relaxation theory recovers macroscopic properties, first-order laminates give too high energy and stresses. (a) Stress–deformation plot, (b) FE simulation using 6400 elements, contour: plastic slip γ, (c) numerical relaxation using $R_1^2 W$.

9.5. Recovery of macroscopic properties

Fig. 12b shows the result of a numerical relaxation for the simple shear problem described above. The corresponding finite element solution is given in Fig. 12a. Note that Fig. 12a was computed with a finite element mesh consisting of 6400 quadrilateral elements consisting of altogether 4×6400 material points, whereas Fig. 12b is obtained at a single material point. The direction and distribution of the laminates can be computed from the optimization variables λ, ρ, α, and β. We like to point out that the relaxed energy approach predicts the volume fractions and the interface orientation but does not predict the number of laminates unless a phase boundary energy is included.

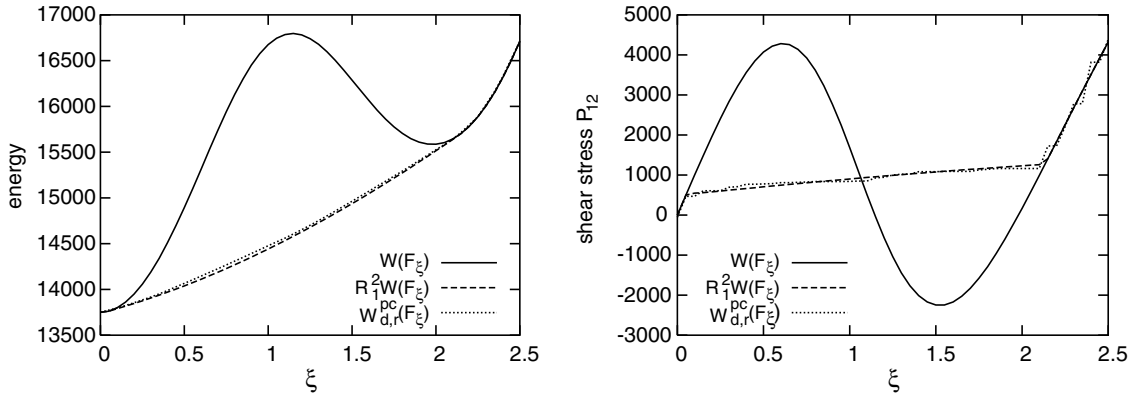

Fig. 15. Energy (a) and first Piola–Kirchhoff shear stress (b) plots for a a simple shear deformation $\mathbf{F}_\xi$ for the energy $W^{\mathrm{red}}_{\gamma_0,p_0}$. Both plots show good agreement of the two relaxation methods.

9.6. Evolution of higher-order laminates

Fig. 13a shows the evolution of the volume fraction λ for the first-order laminate. At each timestep the initial internal parameters $\gamma_0 = p_0 = 0$ had been used, what corresponds to an algorithm with a single-step update of the internal variables. Initially, the material is in a homogeneous elastic state. Then a plastic phase shows up and grows until it reaches 50% volume fraction. At that state the remaining elastic phase becomes plastic, too, but with an opposite plastic slip. Both plastic phases then progress with slowly varying volume fractions. A detailed inspection of the corresponding stress–strain diagram (Fig. 14a) reveals that the stress curve has a slightly negative slope for shear deformations between 0.0 and 0.1. This indicates an unstable behavior and may be caused by an unsatisfying result of the relaxation algorithm using first-order laminates. Indeed, solving the problem with second-order laminates being enabled removes the unsatisfactory negative stress slope: Now, a $N = 3$-type laminate shows up in the first stage of the deformation, comprising an elastic state and a mixture of two opposite-slip plastic states (Fig. 13b). The volume fraction of the elastic phase starts at 100% and then decreases continuously until it vanishes at a deformation of 0.13. The further process coincides with the results of the first-order laminate relaxation. Fig. 14b and c compares the result of the second-order rank-one relaxation with the FE simulation. We observe that both results coincide obviously. It is one of the advantages of the rank-one relaxation that not only an approximate quasiconvex energy, but also information about the volume fraction and shape of the microstructures is obtained.

9.7. Application of two numerical relaxation schemes to $W^{\mathrm{red}}_{\gamma_0,p_0}(F)$

For comparison we apply both numerical approximations introduced in Section 6 to the reduced potential given in 9.5.

Using the algorithm of [8] we iteratively computed the approximation $W^{\mathrm{pc}}_{d,r}(\mathbf{F}_\xi)$ (for $d = 1/16$ and $r = 4$) of $W^{\mathrm{pc}}(\mathbf{F}_\xi)$ and the approximation $R_1^2 W(\mathbf{F}_\xi)$ of $W^{\mathrm{rc}}(\mathbf{F}_\xi)$ for $W = W^{\mathrm{red}}_{\gamma_0,p_0}$ and

$$\mathbf{F}_\xi = \begin{pmatrix} 1.0 & \xi \\ 0.0 & 1.0 \end{pmatrix}$$

with $x = j0.05$ and $j = 0, 1, \ldots, 50$. Fig. 15(a) displays the the unrelaxed energy density $W(\mathbf{F}_\xi)$ and the approximations of the relaxed energies. We observe that $W^{\mathrm{pc}}_{d,r}(\mathbf{F}_\xi)$ and $R_1{}^2W(\mathbf{F}_\xi)$ almost coincide and significantly lower the energy. Therefore, we are tempted to conclude that $W^{\mathrm{pc}}(\mathbf{F}_\xi) = W^{\mathrm{rc}}(\mathbf{F}_\xi)$ and hence $W^{\mathrm{qc}}(\mathbf{F}_\xi) = W^{\mathrm{pc}}(\mathbf{F}_\xi) = W^{\mathrm{rc}}(\mathbf{F}_\xi)$ for $\xi \in [0, 2.5]$. Fig. 15(b) also indicates good agreement of the first Piola–Kirchhoff shear stress obtained from the two numerical relaxations.

It seems surprising that $\mathrm{R}_1^2W(\mathbf{F}_\xi)$ leads to slightly smaller values than $W^{\mathrm{pc}}_{d,r}(\mathbf{F}_\xi)$ since there holds $W^{\mathrm{pc}}(\mathbf{F}_\xi) \leqslant W^{\mathrm{rc}}(\mathbf{F}_\xi)$. The relative difference is however less than 0.01% so that we may assume that this discrepancy is only caused by discretization errors. Notice that the error estimate given in [8] proves that $|\, W^{\mathrm{pc}}_{d,r}(\mathbf{F}_\xi) - W^{\mathrm{pc}}(\mathbf{F}_\xi)\,| \leqslant Cd^2\|D^2W\|_{L^\infty(B_r(\mathbf{0}))}$ and that the discrete polyconvex envelope is a reliable upper bound for the exact polyconvex envelope, i.e. $W^{\mathrm{pc}}_{d,r}(\mathbf{F}_\xi) \geqslant W^{\mathrm{pc}}(\mathbf{F}_\xi)$.

Although the approximate values of the relaxed energies almost coincide, the related Young measures may differ significantly: For $\xi = 0.1$ we obtained the value

$$W^{\mathrm{pc}}_{d,r}(\mathbf{F}_{0.1}) = \sum_{\mathbf{A}\in\mathcal{N}_{d,r}} \lambda_{\mathbf{A}} W(\mathbf{A}) = 13,791.19$$

with convex coefficients (which are larger than $1.0E{-}05$) and gradients

$$\lambda_{\mathbf{A}_1} = 0.1000, \quad \mathbf{A}_1 = \begin{pmatrix} 1.1250 & -0.0625 \\ 0.1875 & 0.8750 \end{pmatrix},$$

$$\lambda_{\mathbf{A}_2} = 0.1250, \quad \mathbf{A}_2 = \begin{pmatrix} 0.8125 & 0.3750 \\ -0.1250 & 1.1875 \end{pmatrix},$$

$$\lambda_{\mathbf{A}_3} = 0.0250, \quad \mathbf{A}_3 = \begin{pmatrix} 0.7500 & 0.5000 \\ -0.1250 & 1.2500 \end{pmatrix},$$

$$\lambda_{\mathbf{A}_4} = 0.2750, \quad \mathbf{A}_4 = \begin{pmatrix} 1.0625 & 0.0625 \\ 0.0000 & 0.9375 \end{pmatrix},$$

$$\lambda_{\mathbf{A}_5} = 0.4750, \quad \mathbf{A}_5 = \begin{pmatrix} 1.0000 & 0.0625 \\ 0.0000 & 1.0000 \end{pmatrix},$$

while the computation of $R_1^2W(\mathbf{F}_{0.1})$ led to the approximation

$$\mathrm{R}_1^2W(\mathbf{F}_{0.1}) = 13,790.53,$$

where the volume fractions and gradients are given by

$$\lambda_{\mathbf{A}_1} = 0.4789, \quad \mathbf{A}_1 = \begin{pmatrix} 0.9853 & 0.1031 \\ -0.0458 & 1.0096 \end{pmatrix},$$

$$\lambda_{\mathbf{A}_{21}} = 0.2451, \quad \mathbf{A}_{21} = \begin{pmatrix} 0.8536 & 0.2570 \\ -0.1066 & 1.1399 \end{pmatrix},$$

$$\lambda_{\mathbf{A}_{22}} = 0.2760, \quad \mathbf{A}_{22} = \begin{pmatrix} 1.1554 & -0.0447 \\ 0.1741 & 0.8591 \end{pmatrix},$$

which constitutes a second-order laminate. Notice that the value of the unrelaxed energy is

$$W(\mathbf{F}_{0.1}) = 13,799.88,$$

so that the difference between $W^{\mathrm{pc}}_{d,r}(\mathbf{F}_{0.1})$ and $R_1^2W(\mathbf{F}_{0.1})$ is much smaller than the reduction of the energy obtained by relaxation.

10. Outlook

This paper presents effective algorithms in relaxation theory for the modeling of microstructure evolution. For specific (convex) relaxed potentials a full error control is achieved for numerical solutions of the associated boundary value problems. In more general situations numerical approximations of specific envelopes are calculated using different algorithms. These are demonstrated to be accurate and efficient enough in order to solve realistic problems in continuum mechanics.

The field of numerical relaxation, however, is still in its infancy. This section reports here on a a few pressing questions for future experimental and theoretical investigations.

10.1. Error control in FEM for non-convex minimization problems

The error control mentioned in this paper relies on the convex situation. In fact, for general polyconvex materials, only weak convergence is known (and follows almost immediately from the direct method of the calculus of variations). The only convergence estimate for global solutions is for uniformly convex energy densities [13]—far too restrictive to model a relaxed energy density. This is a wide open and important field for further research.

10.2. Guaranteed convergence of effective solution algorithms

The positive result of Theorem 4.1 on the convergence of a damped or stabilized Newton–Raphson scheme of Section 4 is limited to the convex case as well. It is in fact essential to have sufficient conditions for global convergence of an outer loop (e.g. from Algorithm 4).

10.3. Existence of solutions in time-evolution problems

A natural implicit time-step discretization is known to allow for generalized solutions. The convergence for smaller and smaller time-steps is less clear. Positive results for Young-measure-valued solutions are reported in [44,18]; the question of Sobolev-valued solutions remains open for non-monotone hyperbolic systems.

10.4. Update of microstructured internal variables

In Sections 8 and 9 we have studied relaxations of the reduced potential $W^{\mathrm{red}}_{\mathbf{K}_0}(\mathbf{F})$, being able to predict the onset and morphology of microstructures by the algorithms introduced. This, procedure, however, makes sense only for a given single time-increment. At the beginning of the subsequent increment, the internal variables $\mathbf{K}_0$ are now results of the relaxation performed in the preceding time-increment. Thus they are given in the form Young-measures now, and it is not clear how they should be updated. Let us now look into this problem a little more closely, see also [36] for mathematical details. Let the internal variables $\mathbf{K}$ be elements of a measurable space $\mathscr{K} \in \mathbb{R}^M$ and let a probability-distribution of internal variables at the beginning of the time-increment be given by a Young-measure $\mu_0 \in \mathrm{YM}(\Omega, \mathscr{K})$, where $\mathrm{YM}(\Omega, \mathscr{K})$ denotes the set of all Young-measures on the domain Ω with values in $\mathscr{K}$.

If $\mu_1 \in \mathrm{YM}(\Omega, \mathscr{K})$ represents the probability-distribution at the end of the time-increment, then (8.4) requires the total dissipation to be minimized by the transition from the first distribution into the second one. This is mathematically expressed by the so-called *Wasserstein-distance*

$$D_{\mathrm{wass}}(\mu_0,\mu_1)=\inf\left\{\int_{\mathscr{K}\times\mathscr{K}} D(\mathbf{K}_0,\mathbf{K}_1)\sigma(\mathrm{d}\mathbf{K}_0,\mathrm{d}\mathbf{K}_1)\colon\ \sigma\in \mathrm{YM}(\Omega,\mathscr{K}\times\mathscr{K}),\right.$$
$$\left.\times\int_{\mathscr{K}}\sigma(\cdot,\mathrm{d}\mathbf{K}_1)=\mu_0,\int_{\mathscr{K}}\sigma(\mathrm{d}\mathbf{K}_0,\cdot)=\mu_1\right\}. \tag{10.1}$$

For a given $\mu\in \mathrm{YM}(\Omega,\mathscr{K})$ we define the *cross-quasiconvex envelope* by

$$W^{\mathrm{qc}}(\mathbf{F},\mu)=\inf\left\{\int_{\mathsf{GL}_+(d)\times\mathscr{K}} W(\bar{\mathbf{F}},\mathbf{K})\gamma(\mathrm{d}\bar{\mathbf{F}},\mathrm{d}\mathbf{K})\colon\ \gamma\in \mathrm{YM}(\Omega,\mathsf{GL}_+(d)\times\mathscr{K}),\right.$$
$$\left.\int_{\mathscr{K}}\gamma(\cdot,\mathrm{d}\mathbf{K})\in \mathrm{GYM}(\Omega,\mathsf{GL}_+(d)),\int_{\mathsf{GL}_+(d)}\gamma(\mathrm{d}\bar{\mathbf{F}},\cdot)=\mu,\int_{\mathsf{GL}_+(d)\times\mathscr{K}}\bar{\mathbf{F}}\gamma(\mathrm{d}\bar{\mathbf{F}},\mathrm{d}\mathbf{K})=\mathbf{F}\right\}, \tag{10.2}$$

$\mathrm{GYM}(\Omega,GL_+(d))$ denoting the set of all Gradient-Young-Measures on the domain Ω with values in $GL_+(d)$.

With this notation it is now possible to generalize the definition of reduced potential given in 8.8 and the update-formula 8.9 in a canonical way to the measure-valued case. We obtain

$$W^{\mathrm{red}}_{\mu_0}(\mathbf{F})=\inf\{W^{\mathrm{qc}}(\mathbf{F},\mu)+D_{\mathrm{wass}}(\mu_0,\mu)\colon\ \ \mu\in \mathrm{YM}(\Omega,\mathscr{K})\} \tag{10.3}$$

and

$$\mu_1=\arg\inf\{W^{\mathrm{qc}}(\mathbf{F},\mu)+D_{\mathrm{wass}}(\mu_0,\mu)\colon\ \ \mu\in \mathrm{YM}(\Omega,\mathscr{K})\}. \tag{10.4}$$

By construction $W^{\mathrm{red}}_{\mu_0}(\mathbf{F})$ is quasiconvex. Hence, we are once again in the well-posed regime concerning the associated boundary value problems. For the purpose of numerical implementation, of course, the general Young-measures above have to be replace by discrete constructions which mostly will have to rely on point-measures. One possible procedure could involve the approximation of $W^{\mathrm{qc}}(\mathbf{F},\mu)$ by a cross-polyconvex envelope.

10.5. Beyond young-measures

Even the approach outlined above has its limitations. Young-measures essentially model probability-distributions, i.e. volume-ratios between different components. Some microstructures, however, require more information to be appropriately described, an example being evolving microcrack-fields in damage-mechanics, where orientation plays a crucial role. A concept to capture such properties would be so-called H-measures [48], defined by Fourier-expansions of deformation-fields; this is restricted to quadratic potentials.

11. Uncited references

[10,26]

Acknowledgment

The support of the DFG through the priority program 1095 "Analysis, Modeling and Simulation of Multiscale Problems", the Austrian Science Fund FWF under grant P15274 and the EPSRC under grant N09176/01 is thankfully acknowledged. Part of this work was done during a visit of three of the four authors to the Isaac-Newton Institute of Mathematical Sciences, Cambridge, England.

References

[1] S. Aubry, M. Fago, M. Ortiz, A constrained sequential-lamination algorithm for the simulation of sub-grid microstructure in martensitic materials, Comput. Methods Appl. Mech. Engrg. 192 (26–27) (2003) 2823–2843.

[2] J.M. Ball, Convexity conditions and existence theorems in nonlinear elasticity, Arch. Rational Mech. Anal. 63 (4) (1977) 337–403.

[3] J.M. Ball, Strict convexity, strong ellipticity, and regularity in the calculus of variations, Math. Proc. Cambridge Philos. Soc. 87 (3) (1980) 501–513.

[4] J.M. Ball, A version of the fundamental theorem for Young measures. in: Partial Differential Equations and Continuum Models of Phase Transitions, M. Rascle, D. Serre, M. Slemrod (Eds.), Lecture Notes in Physics, vol. 344, 1989, pp. 207–215.

[5] J.M. Ball, R.D. James, Fine phase mixtures as minimizers of energy, Arch. Rational Mech. Anal. 100 (1987) 13–52.

[6] J.M. Ball, B. Kirchheim, J. Kristensen, Regularity of quasiconvex envelopes, Calc. Var. Partial Differ. Equat. 11 (2000) 333–359.

[7] S. Bartels, C. Carstensen, P. Plecháč, A. Prohl, Convergence for stabilisation of degenerately convex minimisation problems, Interfaces and Free Boundaries 6 (2) (2004) 253–269.

[8] S. Bartels, Reliable and efficient approximation of polyconvex envelopes, Preprints of the DFG Priority Program "Multiscale Problems" 76 (2003). Available from: <www.mathematik.uni-stuttgart.de/~mehrskalen/>.

[9] S. Bartels, A. Prohl, Multiscale resolution in the computation of crystalline microstructure, Numer. Math. 96 (4) (2004) 641–660.

[10] S.C. Brenner, L.R. Scott, The mathematical theory of finite element methodsTexts in Applied Mathematics, vol. 15, Springer-Verlag, New York, 2002, p. xvi+361.

[11] O. Bolza, A fifth necessary condition for a strong extremum of the integral $\int_{x_0}^{x_1} f(x,y,y')\mathrm{d}x$, Trans. Am. Math. Soc. 7 (2) (1906) 314–324.

[12] C. Carstensen, All first-order averaging techniques for a posteriori finite element error control on unstructured grids are efficient and reliable, Math. Comp. 73 (247) (2004) 1153–1165.

[13] C. Carstensen, G. Dolzmann, An a priori error estimate for finite element discretizations in nonlinear elasticity for polyconvex materials under small loads, Numer. Math. 97 (1) (2004) 67–80.

[14] C. Carstensen, K. Hackl, On microstructures occurring in a model of finite-strain elastoplasticity involving a single slip-system, ZAMM 80 (2) (2000) S421–S422.

[15] C. Carstensen, K. Hackl, A. Mielke, Nonconvex potentials and microstructures in finite-strain plasticity, Proc. R. Soc. Lond. A 458 (2018) (2002) 299–317.

[16] C. Carstensen, K. Jochimsen, Adaptive finite element methods for microstructures? Numerical experiments for a 2-well benchmark, Computing 71 (2003) 175–204.

[17] C. Carstensen, R. Klose, A posteriori finite element error control for the p-Laplace problem, SIAM J. Sci. Comput. 25 (3) (2003) 792–814.

[18] C. Carstensen, M.O. Rieger, Young-Measure approximations for elastodynamics with non-monotone stress-strain relations, M2AN Math. Model. Numer. Anal. 38 (3) (2004) 397–418.

[19] C. Carstensen, S. Müller, Local stress regularity in scalar non-convex variational problem, SIAM J. Math. Anal. 34 (2) (2002) 495–509.

[20] C. Carstensen, P. Plecháč, Numerical solution of the scalar double-well problem allowing microstructure, Math. Comput. 66 (219) (1997) 997–1026.

[21] C. Carstensen, P. Plecháč, Numerical analysis of compatible phase transitions in elastic solids, SIAM J. Numer. Anal. 37 (6) (2000) 2061–2081.

[22] C. Carstensen, P. Plecháč, Numerical analysis of a relaxed variational model of hysteresis in two-phase solids, M2AN Math. Model. Numer. Anal. 35 (5) (2001) 865–878.

[23] M. Chipot, S. Müller, Sharp energy estimates for finite element approximations of non-convex problems. Variations of domain and free-boundary problems in solid mechanics (Paris, 1997), Solid Mech. Appl., 66, Kluwer Acad. Publ., Dordrecht, 1991.

[24] B. Dacorogna, Direct methods in the calculus of variations, Springer-Verlag, Berlin, 1989.

[25] G. Dolzmann, Numerical computation of rank-one convex envelopes, SIAM J. Numer. Anal. 36 (5) (1999) 1621–1635.

[26] J. Goodman, R.V. Kohn, L. Reyna, Numerical study of a relaxed variational problem from optimal design, Comput. Methods Appl. Mech. Engrg. 57 (1) (1986) 107–127.

[27] K. Hackl, Generalized standard media and variational principles in classical and finite strain elastoplasticity, J. Mech. Phys. Solids 45 (5) (1997) 667–688.

[28] K. Hackl, U. Hoppe, On the calculation of microstructures for inelastic materials using relaxed energies, in: C. Miehe (Ed.), IUTAM Symposium on Computational Mechanics of Solid Materials at Large Strains, Solid Mechanics and its Applications, 108, Kluwer, 2003, pp. 77–86.

[29] B. Halphen, Q.S. Nguyen, Sur les matériaux standards géneralises, J. Mech. 14 (1975) 39–63.

[30] D. Kinderlehrer, P. Pedregal, Weak convergence of integrands and the Young measure representation, SIAM J. Math. Anal. 23 (1991) 1–19.

[31] R.V. Kohn, The relaxation of a double-well energy, Contin. Mech. Thermodyn. 3 (3) (1991) 193–236.